DESIGN & DEVELOPMENT OF 3 DOF AUTONOMOUS UNDERWATER BUOYANCY DRIVEN VEHICLE

A Final Year Project Report

Presented to

SCHOOL OF MECHANICAL & MANUFACTURING ENGINEERING

Department of Mechanical Engineering

NUST

ISLAMABAD, PAKISTAN

In Partial Fulfillment
of the Requirements for the Degree of
Bachelors of Mechanical Engineering

---

by

Muhammad Sumran Shahid

Muhammad Bilal Siddique

Muhammad Muneeb Ahmad

Hamza Bin Umar

June 2024

EXAMINATION COMMITTEE

We hereby recommend that the final year project report prepared under our supervision by:

Muhammad Sumran Shahid	334951
Muhammad Bilal Siddique	331548
Muhammad Muneeb Ahmad	331217
Hamza Bin Umar	346734

Titled: "Design and Development of 3 DoF Autonomous Underwater Buoyancy Driven Vehicle" be accepted in partial fulfillment of the requirements for the award of BS Mechanical Engineering degree with grade ___

Supervisor: Dr. Saad Ayub Jajja, Assistant Professor

Dated: 4th July 2024

(Head of Department)

4-7-24

(Date)

COUNTERSIGNED

Dated: 4-7-24

(Dean / Principal)

ABSTRACT

The "Design and Development of 3 DoF Underwater Buoyancy Driven Vehicle" project aims to create a new kind of underwater vehicle that can move in all directions using buoyancy as its power source. This report covers everything we've done and achieved during the project. At the start, we used computer simulations to make sure the vehicle would move well in water and stay structurally sound. We also did lots of math to figure out things like how strong the motor needed to be and how to make sure everything stayed watertight. Then, we used computer models to keep improving the design until it was just right for making real prototypes. We made sure to get all the parts we needed on time, so we could put everything together and test it out. Our goal is to make a tough, efficient underwater vehicle that can handle all kinds of challenges in the water.

TABLE OF CONTENTS

LIST OF TABLES

LIST OF FIGURES

ABBREVIATIONS

AUV	Autonomous Underwater Vehicle
CFD	Computation Fluid Dynamics
FEA	Finite Element Analysis
ROV	Remotely Operated Vehicle
CG	Centre of Gravity
CB	Centre of Buoyancy
UPVC	Unplasticized Poly Vinyl Carbonate
VB	Variable Buoyancy
ITTC	International Towing Tank Conference

NOMENCLATURE

U	Velocity
α	Angle of attack
β	Angle of incidence
u	Upstream velocity
p	Pressure
k	Turbulent kinetic energy
ω	Specific dissipation of turbulent kinetic energy
ξ_B	Parameter direction crossing the boundary
F_B	Buoyancy Force
ρ	Density
g	Gravitational Acceleration
G_d	O-Ring groove diameter
B_d	O-Ring base diameter

CHAPTER 1: INTRODUCTION

The vastness and complexity of the world's oceans demand innovative technologies for efficient exploration. While conventional propeller driven underwater vehicles play a crucial role, their limitations in range and endurance present challenges for comprehensive studies. In this context, underwater buoyancy-driven vehicles offer a novel and transformative approach. This report delves into the intriguing world of Buoyancy-driven vehicles, unveiling their operational mechanisms and their potential to reshape oceanic exploration.

Buoyancy-driven vehicles operate on a captivating principle by harnessing the power of buoyancy and gliding. Through intricate mechanisms, they adjust their volume, achieving efficient forward motion without propellers. This report dissects the inner workings of Buoyancy-driven vehicles, examining their buoyancy control systems, hydrofoil designs, and gliding dynamics.

Firstly, Buoyancy-driven vehicles boast significantly extended range and endurance thanks to their low energy consumption. Unlike propeller-driven counterparts, they leverage gravity and lift to glide effortlessly through the water, minimizing energy expenditure. This translates to vastly extended operational capability, enabling Buoyancy-driven vehicles to undertake missions spanning weeks or even months, covering thousands of kilometers.

Secondly, Buoyancy-driven vehicles offer a paradigm shift in data collection patterns. Their unique "sawtooth" movement patterns allow them to gather information at multiple depths, providing valuable insights into dynamic oceanographic processes and temporal changes that would be impossible to capture with traditional methods.

The report presents the diverse applications of Buoyancy-driven vehicles, encompassing oceanographic research, climate monitoring, underwater resource

exploration, and defense operations. By harnessing the power of buoyancy and gliding, they offer a shift in underwater exploration, opening doors to a deeper understanding of our planet's hidden aquatic realm.

Historically, ocean exploration relied on conventional methods with research vessels and moored observatories. However, limitations in cost and scalability hindered widespread data collection. The advent of satellite-based technologies marked a transformative era, enabling the development of cost-effective Autonomous Underwater Vehicles (AUVs), Remotely Operated Vehicles (ROVs), and Autonomous Underwater Gliders (AUGs).

CHAPTER 2: LITERATURE REVIEW

Historically, the exploration of the ocean's depths primarily relied upon conventional methods, which included the deployment of instruments from research vessels or the installation of moored observatories. Research expeditions conducted aboard ships ranged durations from one to several months, while moorings, designed to endure the ocean's rigors, could remain in place for up to a year or more. However, these established observation platforms posed significant challenges and required substantial costs, limiting their multiplication and hence, the scope of ocean data collection efforts.

The emergence of satellite-based navigation and communication technologies introduced in a transformative era in oceanography. These advancements facilitated the way for the development of a novel class of small, cost-effective instrument platforms, which are reshaping the landscape of ocean observation. Among the most notable contributors to this significant change are Autonomous Underwater Vehicles (AUVs), Remotely Operated Vehicles (ROVs), and Autonomous Underwater Gliders (AUGs). These autonomous platforms have emerged as critical players in marine environmental data acquisition, promoting advancements in our understanding of the oceans.

In the world of Autonomous Underwater Vehicles (AUVs) and Autonomous Underwater Gliders (AUGs), some important concepts to know are their working principles, operating characteristics, and diverse applications. It further examines the concepts of buoyancy generation, hydrodynamic performance, and gliding control, which

helps to understand the mechanisms that propel these submersible technologies through the ocean's depths. The following sections explore the literature about their design and development, hydrodynamic analyses, and the evolution of variable buoyancy systems. By understanding the dynamic forces that govern the movement of these gliders, we gain a comprehensive understanding of their capabilities. This also aims to critically evaluate the contributions to oceanographic research and provides insights into the objectives and scope of this exploration.

2.1 Design and Development:

Stommel (1989) first talked about the idea of an underwater glider. As of today, three primary types of AUGs exist:

- Electric Gliders: These AUGs employ battery-powered pumps to control buoyancy. Webb et al. (2001) discussed the design details and field trials of Slocum electric gliders, explaining their operational capabilities and limitations.
- Thermal Gliders: this type of AUG harnesses energy from the ocean's temperature gradient. Webb et al. (2001) provided insights into the design and operation of Slocum thermal gliders, emphasizing their unique approach to propulsion.
- Hybrid Gliders: Hybrid AUGs combine battery-powered propellers for propulsion with battery-powered pumps for buoyancy control. These are versatile gliders and offer a balance between energy efficiency and propulsion power.

Webb et al. (2001) explained the details and results of testing Slocum electric and thermal gliders. Eriksen et al. (2001) shared information about the development and use of Seaglider. Sherman et al. (2001) discussed Spray glider's development and field test results.

Davis et al. (2002) compared different commercial gliders. Rudnick et al. (2004) looked at Slocum, Spray, and Seaglider designs for ocean research.

There are already tested underwater gliders like Slocum, Seaglider, Spray, Slocum thermal, X-Ray, and Deep glider in oceanographic research and littoral survey missions. Slocum, Spray, and Seaglider are called 'legacy gliders,' and there are more designs following their footsteps.

Table 2.1: Characteristics of Underwater Gliders

Glider name	**Max. depth (m)**	**Speed (m/s)**	**Range (km)**	**Batteries (MJ)**	**Mass (kg)**	**Hull and fairing**	**Wings**
Slocum	200	0.25 m/s horizontal, Glide angle= 20°	2300	260 Alkaline C cells, 8 MJ	51	Length = 1.5m Diameter= 21.3 cm	Span=98cm, Chord=14cm , 45° sweep back
Spray	1500	0.25 m/s horizontal, Glide angle= 18°	7000	2 Lithium CSC DD cells, 13 MJ	52	Length = 2m Diameter=20cm	Span=120cm , Chord=10cm
Seaglider	1000	0.25 m/s horizontal, Glide angle= 18°	4500	81 Lithium D cells, 10 MJ	51	Length = 1.8m, Diameter=30cm	Span=100cm , Chord=16cm

2.2 Hydrodynamic Analysis:

Hydrodynamic design studies how gliders move in water, looking at factors like drag, lift to drag ratio, and stability. Researchers use model experiments and computer simulations (CFD) for this.

Geisbert et al. (2007) checked hydrodynamic parameters for Slocum, X-Ray, and Virginia Tech miniature AUV. Dong et al. (2008) made a simulation program for pitch control using CFD for AUG development. Ichihashi et al. (2008) used CFD for hydrodynamic forces estimation for 'Alex' glider. Jianguo et al. (2011) did CFD analysis for the 'Petrel' glider. Ting et al. (2012) looked into hydrodynamic characteristics using CFD. Zhang et al. (2012) applied CFD in designing an AUG glider. Zhang et al. (2013)

used CFD for hydrodynamic coefficients of 'Seawing' glider to simulate its spiraling motion.

2.3 Development of Variable Buoyancy Systems:

Variable buoyancy (VB) helps underwater vehicles save energy. Bagley et al. (2005) proposed a buoyancy control system. Worall et al. (2007) created a VB engine for deepwater vehicles. Tangirala et al. (2007) developed a VB engine and control software for AUV 'Seahorse.' Zhao et al. (2010) made a bladder-based VB engine for a long-range AUV. Wang et al. (2011) gave formulations for designing VB engines based on AUV operational depth.

2.4 Glider Dynamics:

Understanding how gliders move is important for predicting their performance, designing better control, developing advanced control and navigation algorithms, and refining their design. Researchers have conducted extensive studies in this domain, aiming to enhance glider motion performance.

Graver et al. (1998) delved into the design and preliminary analysis of a small underwater vehicle, specifically created for testing and demonstrating gliding dynamics.

Leonard and Graver (2001) proposed equations of motion for gliders in the vertical plane, facilitating model-based feedback control algorithms.

Graver (2005) developed dynamic models for gliders, subsequently applied in the analysis of glider control, navigation, and design.

Mahmoudian (2009) presented a numerical implementation of a feedback/feedforward control algorithm, offering improved motion performance for gliders.

Yang et al. (2013) built a prototype glider based on a dynamic model, validating its performance through experimental results.

2.5 Working Principle:

Autonomous underwater vehicles (AUV) operate on the principle of combined buoyancy control and hydrodynamic forces for precise oceanic navigation.

The AUV is equipped with a ballast system, typically consisting of ballast tanks or chambers that can be filled with or emptied of water. To initiate movement, the AUV adjusts its buoyancy by controlling the amount of water in the ballast system. By expelling water from the ballast tanks, the vehicle becomes less dense, leading to positive buoyancy and ascent. Similarly, taking in water increases density, resulting in negative buoyancy and descent.

2.5.1 Vertical Motion: The AUV controls its vertical motion by precisely regulating the buoyancy changes. To descend, the ballast system allows the intake of water, increasing the vehicle's weight. For ascent, the expulsion of water decreases weight, facilitating upward movement.

This buoyancy control is a dynamic process, enabling the AUV to navigate through various depths in the water column with precision.

2.5.2 Horizontal Propulsion: The horizontal propulsion of the AUV is achieved by utilizing the buoyancy control system in a strategic manner. To move forward, the AUV may tilt slightly downward, directing its forward motion. By adjusting the buoyancy and pitch angle, the vehicle generates a controlled horizontal glide.

The sawtooth profile of the AUV's trajectory during ascent and descent is a characteristic feature resulting from the combined effects of buoyancy changes and hydrodynamic forces.

Figure 2.1: Sawtooth Profile of AUVs

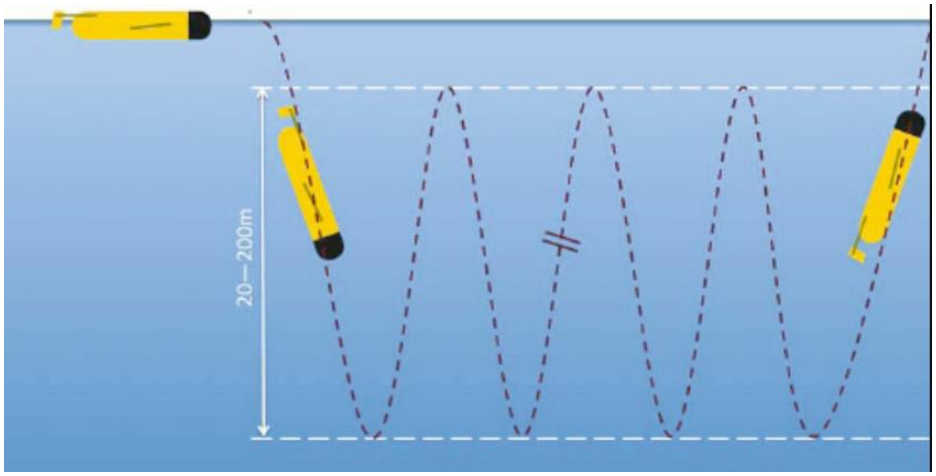

2.5.3 Steering and Maneuvering: Initiating fluid movement within the ballast chamber, achieves precise buoyancy adjustments, accompanied by pitching effects. Batteries which act as a moving mass, fine-tune pitch angles. Steering and maneuvering are achieved by modulating the buoyancy control system to induce controlled pitch, roll, and yaw movements.

2.5.4 Buoyancy Control: Buoyancy control is achieved by altering the glider's displaced volume. Various methods exist for controlling buoyancy in gliders. Reciprocating hydraulic pumps, as used in Spray and Seaglider, inflate and deflate a bladder with hydraulic oil to adjust the glider's buoyancy. While these devices are compact and lightweight, their design is relatively complex, involving valves and plumbing, and they are susceptible to issues like vapor lock at high pressures. Such mechanisms are most suitable for deep-sea gliders [Geisbert, 2007]. Single-stroke piston pumps rely on gearing to achieve high mechanical advantage for buoyancy control, making them preferable for shallow-water operations where rapid maneuverability and good two-way buoyancy

control are crucial. However, this method is challenging for deep-sea, high-pressure operations [Graver et al., 1998].

Figure 2.2: Reciprocating Hydraulic Pump

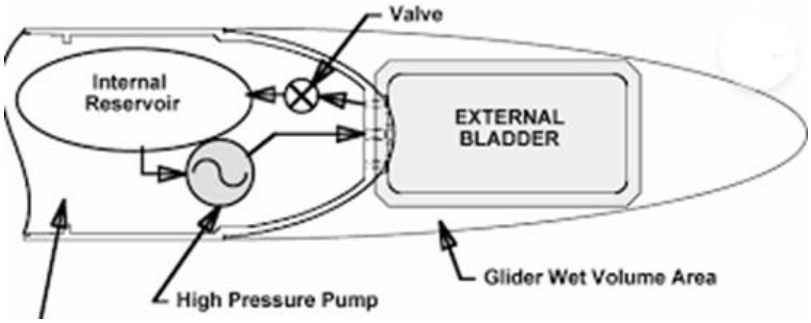

2.5.5 Pitch Control: Pitch, influencing dive angle, is typically controlled by shifting an internal mass forward and backward within the glider. In most cases, this internal mass comprises batteries on a movable sled. Some gliders may achieve the necessary pitching moment by locating the bladder or variable ballast at the glider's nose. Fine control of the pitch angle is then accomplished by adjusting the internal mass.

Figure 2.3: Pitch Control using moving mass

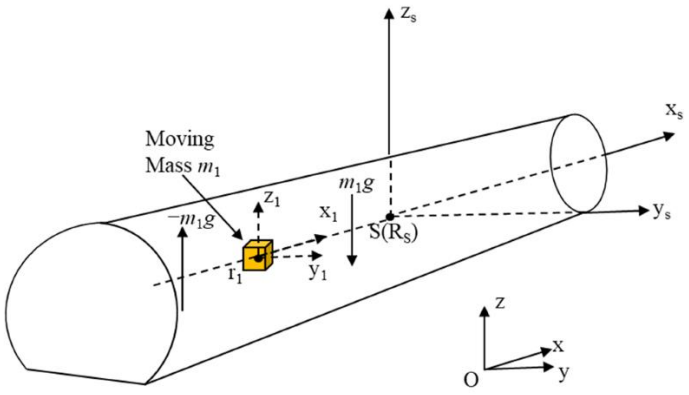

2.5.6 Heading Control: Two methods are currently employed for heading control. The more intuitive method involves deflecting a rudder to induce a yawing moment. A less intuitive approach is to rotate an eccentric mass around the glider's longitudinal axis,

causing it to roll and allowing a component of the lift force to act laterally, producing a spiral motion. Gliders that roll to turn achieve a turning radius of 20 to 30 meters, while those using rudders are better suited for shallow operations, offering a tighter turning circle of about 7 meters [Davis et al., 2002].

2.6 Operating Characteristics:

Autonomous Underwater Gliders (AUGs) possess distinct operating characteristics crucial for excelling in oceanographic research and environmental monitoring. The glider's trajectory, propulsion mechanisms, and data collection capabilities are integral components.

The operational principles of underwater gliders are analogous to sailplanes. Glider wings generate lift forces perpendicular to the glide path, allowing the glider to convert buoyancy into horizontal motion. This lift force overcomes the drag force, propelling the glider forward.

Gliders primarily employ buoyancy for propulsion. Energy for gliding is predominantly supplied at the bottom of each dive cycle, where work is done to increase the vehicle's volume, making it positively buoyant. At the apex of each dive cycle, the vehicle's volume is decreased to attain negative buoyancy. By executing a series of downward and upward glides, gliders induce horizontal translation during their sawtooth glide (Figure 1). Operating at relatively low speeds makes gliders more efficient than faster submersibles, albeit at the expense of speed and maneuverability. This trade-off enables the long-range deployments observed in the current generation of underwater gliders [Graver, 2005].

2.6.1 Buoyancy Generation:

The trajectory of an AUG is defined by its sawtooth operating pattern, driven by buoyancy control. Lift force from wing-generated vertical motion propels the glider forward. Electric or thermal energy is converted into pressure-volume work, altering buoyancy and creating thrust. The sawtooth profile covers a wide spatial area, ensuring comprehensive data acquisition. Variants like 'Slocum thermal' use temperature differences for power.

Figure 2.4: Forces acting on an AUV

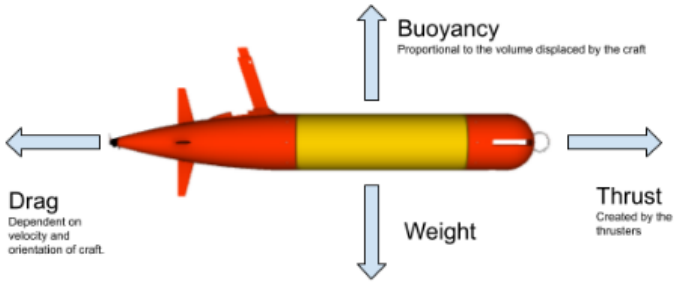

2.6.2 Hydrodynamic Performance:

AUGs exhibit efficient, slow-speed gliding with low drag, optimizing range and duration. High lift-to-drag ratios, critical for deep-sea operations, result from wing design. Hulls manage buoyancy variations, preventing significant shifts. Variable buoyancy systems enhance gliding velocity, with bladder-based systems for deep-sea and single-stroke pump-based systems for shallow waters.

Figure 2.5: Hydrodynamic Profile

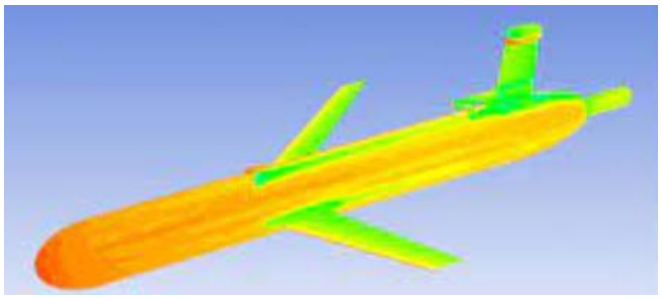

2.6.3 Gliding Control:

Buoyancy, pitch, and heading control systems govern glider motion. Buoyancy control adjusts mass flow or piston frequency, inducing pitching. Pitch control involves shifting internal mass for precise angle adjustments. Heading control uses rudder deflection for yaw or eccentric mass rotation for rolling. Operational environments dictate control methods, with rolling-based suited for deep-sea and rudder-based for shallow waters.

Figure 2.6: Glider Movement

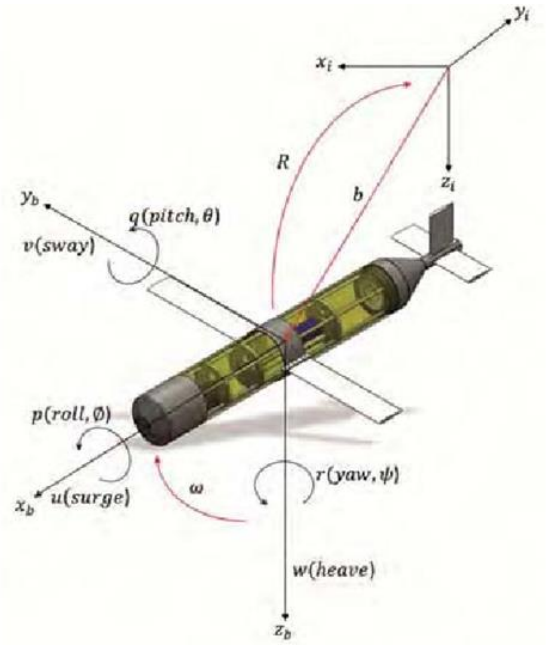

2.7 Modern Underwater Gliders:

Presently, three well-known underwater glider designs are widely utilized: Slocum [Webb et al., 2001], Spray [Sherman et al., 2001], and Seaglider [Eriksen et al., 2001]. Table 1 outlines the distinctions among these current glider designs, summarizing information sourced from [Davis et al., 2002] and [Rudnick et al., 2004].

Spray and Seaglider are crafted for maximum depths ranging from 1000 to 2000 meters. These gliders are optimized for minimal energy consumption, reduced drag,

extended range, and prolonged mission duration. In contrast, the Slocum Electric is designed for shallow operations with a maximum depth of only 200 meters. Its primary focus is on maneuverability for coastal and tidal environments rather than extended range.

Each of these three distinctive underwater glider designs: Slocum Battery, Spray, and Seaglider AUVs has been engineered with unique characteristics and mission profiles, catering to specific operational requirements and environmental conditions.

1. **Slocum:**

Originating in 1978 at Woods Hole Oceanographic Institution, the Slocum glider's design evolved for shallow coastal operations, excelling in rapid turning and vertical velocity changes. Using thermal energy from the thermocline for propulsion, Slocum features a shallow pressure rating, large-volume pump, and efficient volume control. Pitch adjustments utilize internal mass shifts, and an air bladder enhances surface buoyancy. Integrated antennas in a vertical stabilizer aid navigation and communication.

Figure 2.7: Slocum Electric

2. **Spray:**

Drawing inspiration from Henry Stommel's vision, the Spray glider prioritizes energy efficiency for long-duration, deep-ocean missions. Its fine entry hull shape reduces drag, employing a high-pressure pump for hydraulic propulsion. During navigation, antennas are stowed in a rotating wing, and the vertical stabilizer includes an emergency-recovery

antenna. Glide and pitch control are achieved through internal battery pack translation and rotation, with turning initiated by controlled rolling for enhanced directional changes.

Figure 2.8: Spray

3. Seaglider:

Developed in the early 2000s at the University of Washington, Seaglider is a versatile AUV designed for long-duration, autonomous missions, contributing significantly to oceanographic research. Encased in a low-drag hydrodynamic fiberglass fairing, Seaglider maximizes laminar boundary layer retention. Its neutrally compressible hull conserves buoyant driving force during depth changes. Utilizing a hydraulic system for buoyancy control, Seaglider exhibits remarkable maneuverability, featuring turning dynamics opposite to those of Spray.

Figure 2.9: Sea Glider

2.7.1 Localization Methods Used in Modern Gliders

Information regarding how Slocum, Spray, and Seaglider navigate is outlined in the 2001 series of articles published in the IEEE Journal of Oceanic Engineering [Webb et al., 2001; Sherman et al., 2001; Eriksen et al., 2001].

Slocum does not estimate water currents. Navigation involves calculating heading and glide angles between GPS fixes on the surface, maintained during dives. The glider dead reckons while submerged using heading, vertical velocity, pitch, and buoyancy [Webb et al., 2001].

Similarly, Spray employs a simple navigation algorithm to compute heading and dive angles needed to reach a desired location from its current position. It neglects currents, assuming constant pitch, heading, and angle of attack during transit [Sherman et al., 2001].

Seaglider stands out by estimating water currents using a Kalman filter. This filter fuses actual surface positions and those projected by dead reckoning during dive cycles to estimate water currents [Eriksen et al., 2001]. Target heading and glide angle are adjusted to compensate for the estimated water currents, minimizing power consumption and ensuring accurate target destination approach.

2.8 Applications of AUG:

Autonomous Underwater gliders (AUGs) have become important tools in the field of scientific and defense/naval domains, and are used in a wide range of applications across various industries, some of which are:

1. Oceanography Research and Surveys:

Moored instruments, also known as moored oceanographic instruments, are scientific instruments that are deployed in the ocean and anchored to the seafloor or a fixed point in the water column using a mooring system. Moored instruments are used to gather

continuous and precise data about various oceanic parameters over long periods of time. They are crucial in oceanographic research, climate studies, and environmental monitoring.

- **Temperature Profiling:** AUGs collect precise temperature data at different ocean depths, which helps human understanding of ocean thermal structure and its impact on weather patterns and climate change.
- **Salinity Measurement:** By measuring conductivity, and hence salinity, AUGs provide critical information about the distribution and variability of salt content in the ocean. This data is important for studying ocean circulation and its role in global climate.
- **Current Speed and Direction:** AUGs track ocean currents, providing valuable insights into their patterns and variations.
- **Depth Profiling:** AUGs offer depth measurements, used for navigation, resource exploration, and hazard assessment.
- **Optical and Acoustic Data:** AUGs can capture data related to optical backscatter, acoustic backscatter, and chlorophyll fluorescence. These measurements are important for studying underwater ecosystems, pollution levels, and marine biodiversity.

2. Defense and Security:

In the defense and naval sectors, AUGs have a wide range of applications, contributing to maritime intelligence, surveillance, and reconnaissance (ISR). Some key uses include:

- **Mine Detection:** AUGs are employed for mine detection operations, as they are silent and their autonomous operation allows them to stealthily search for underwater mines.

- **Antisubmarine Warfare (ASW):** AUGs assist in ASW efforts by detecting, tracking, and monitoring submarines. They can operate covertly, making them effective tools for maintaining naval superiority.Command, Control, and Communications (C3): AUGs support real-time C3 operations by providing data on underwater conditions, enhancing decision-making capabilities for naval commanders.
- **Harbor Patrolling:** AUGs are used for patrolling harbors and coastal areas, ensuring security against potential threats or unauthorized vessels.

3. Environmental Monitoring:

- **Pollution Detection:** Gliders can detect and track pollutants in coastal waters and offshore regions, including oil spills, chemical contaminants, and marine debris, supporting environmental monitoring.
- **Habitat Mapping:** They are used to map and monitor marine habitats such as coral reefs, and seagrass beds, to facilitate habitat conservation.

4. Oil and Gas Industry:

- **Pipeline Inspection:** AUVs and AUGs equipped with sensors and cameras can inspect underwater pipelines for leaks, corrosion, and structural integrity, enhancing the safety and efficiency of oil and gas operations.
- **Exploration:** These vehicles can assist in offshore oil and gas exploration by surveying potential drilling sites, collecting geological data, and examining seabed conditions.

5. Fisheries Management:

Gliders contribute to fisheries management by monitoring fish populations, identifying spawning grounds, and assessing fish abundance and distribution, helping to establish sustainable fishing practices.

6. Search and Rescue Operations:

Gliders can be deployed in search and rescue missions to locate missing vessels, aircraft, or individuals in maritime emergencies, assisting coast guards and rescue teams in coordinating effective response efforts.

Figure 2.10: Applications of AUVs

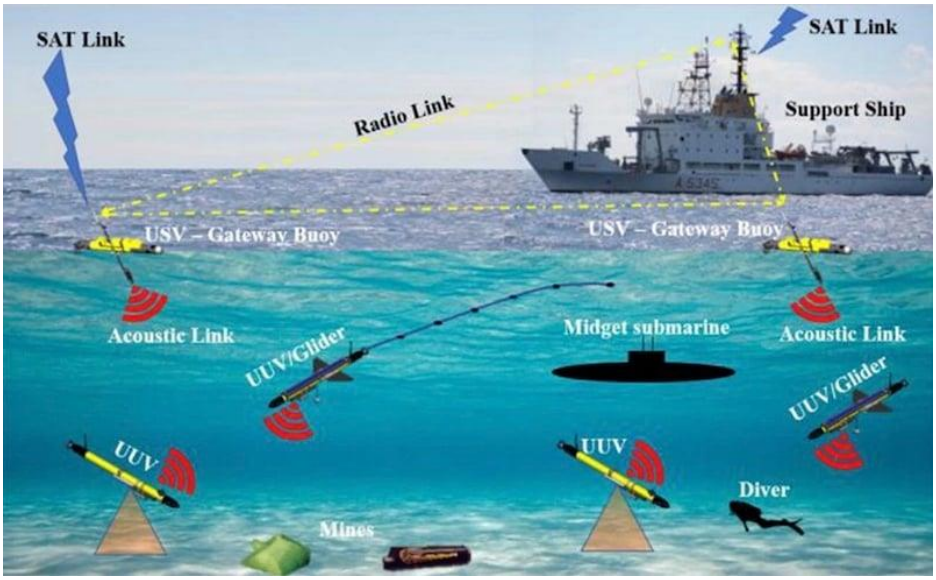

CHAPTER 3: CFD SIMULATION ANALYSIS

The objective of this chapter is to establish a CFD methodology for the computation of the drag and lift forces on the glider. The behaviour of these forces gives the hydrodynamic coefficients of the glider that are essential to understand its behaviour in experimental scenarios. The three coefficients studied in this chapter are the drag, lift and pitching moment coefficients on the glider body. An accurate estimation of the hydrodynamic coefficients of the model is necessary for proper study of the performance of the glider in experimental scenarios.

3.1 Glider Size & Shape Parameters

The hydrodynamic forces on a glider depend on the smoothness and curvature of its whole body (forebody, afterbody and the wings as well). The wings provide the lift force that is required for the forward motion of the glider. For our simulation study, we have taken into consideration the design model 'Alex' by Ichihashi et al. (2008), and modified it to some extent, namely the length, and width of a few components, and modeled it for our own simulations. The design particulars of our simulation model glider are presented in the Table.

Table 3.1: Design particulars of the simulation glider

Length	Hull	0.87 m
	Nose	m
	Tail	0.15 m
	Total	1.12 m
Width (wing span)		0.8 m

Height (including rudders)	0.25 m
Width of body (Hull diameter)	0.1 m
Wing profile	NACA 0009
Rudder profile	NACA 0012
Operation speed	0.5 to 1 m/s
Operation depth	5 m

The 3D CAD model of the simulation glider was developed in the software Solidworks and then imported into ANSYS for CFD simulation in a step file. The following figure shows the dimensions of the model made for CFD analysis.

Figure 3.1: Dimensions of glider model for CFD analysis

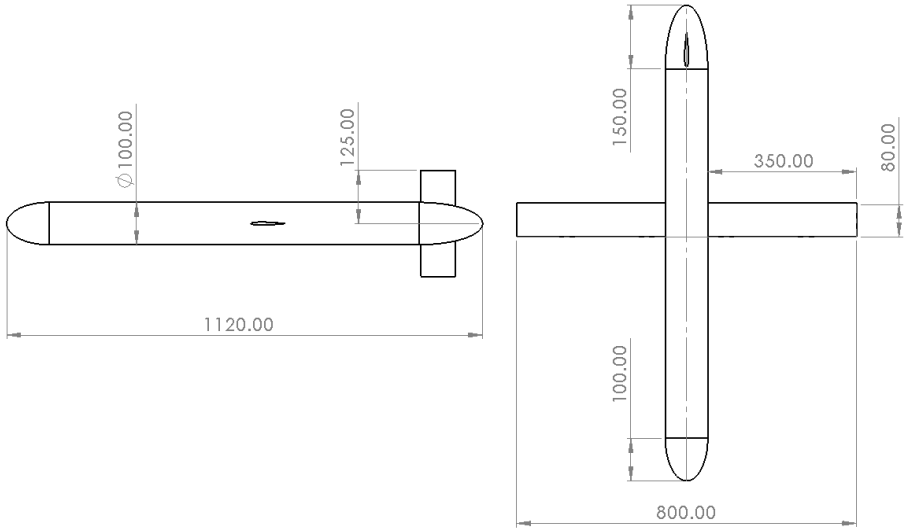

3.2 Towing Tank Test

The Towing Tank Test is a method used in naval architecture and marine engineering to evaluate the hydrodynamic performance of ship and submersible designs. It involves a setup for the measurement of three component forces on a body moving in water, i.e., lift, drag and pitching moment. This test is an important basis for developing the

computation domain for the CFD simulations. The test itself is not within the scope of this project but some specifics of the test are mentioned below to help in developing the computational domain in the next section.

The dimensions of the tank are (Length x Width x Depth =) 6m x 1.5 m x 1 m. The lift and drag forces in the following two cases are measured for flow velocity (U) varying from 0.5 m/s to 1 m/s in steps of 0.1 m/s with (a) angle of the main wings (with the body) at 0^o and angle of attack of the body (α) is changed from -8^o to 8^o in steps of 2^o and (b) angle of the body with respect to its velocity is kept 0 and angle of the main wings with the body (angle of incidence, β) is changed from -8^o to 8^o in steps of 2^o. The arrangement of the experiment in the test is shown in the following figure.

Figure 3.2: Experimental setup for towing tank test (from Ichihashi et al., 2008)

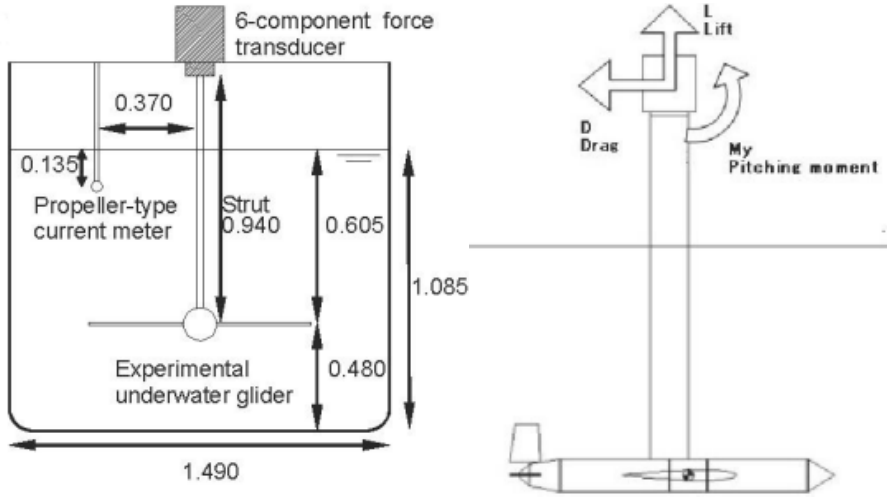

3.3 Computation Domain & Discretization

The computation domain ABCD around the glider is shown in Figure 3.3. $L_f = 5L$, $L_a = L_h = 1.3L$. The downstream length is kept large to observe the wake and turbulent region. The domain also extends to 1.3L in the z region perpendicular to the observation plane. The domain extents are taken in accordance with the ITTC (International Towing Tank Conference) 2011 recommendations for marine CFD applications. The domain around the body is discretized using unstructured meshing. For computational efficiency and stability of the solution, the mesh is kept dense in areas where the flow velocities are sensitive to grid spacing and coarse in other areas. Also, using the technology in Fluent solver of ANSYS, the unstructured tetragonal mesh is converted to Hexahedral mesh to reduce the number of elements and increase the computational speed in limited resources. The final mesh is shown in Figure 3.4.

Figure 3.3: Computational domain for glider CFD with boundary conditions

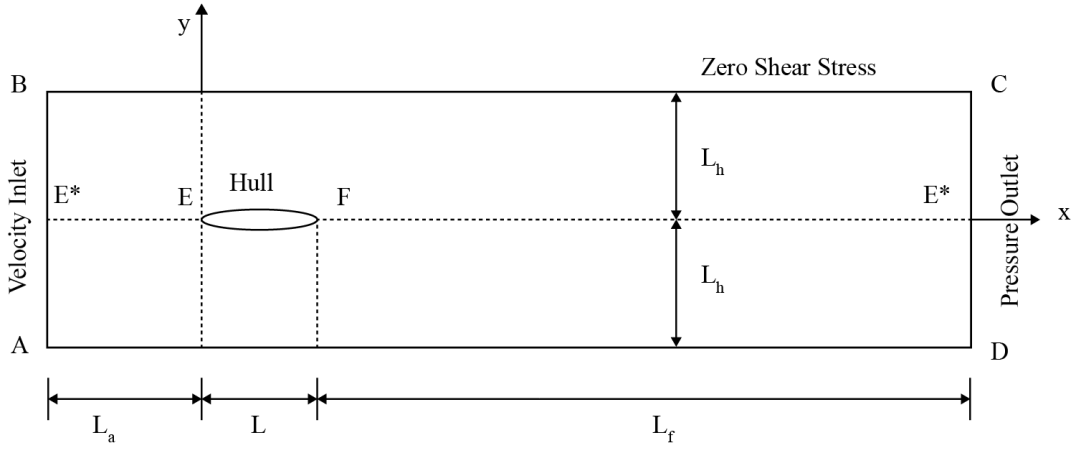

Figure 3.4: Distribution of unstructured cells around the model; tetrahedral and hexahedral
(No. of cells = 1.1 million)

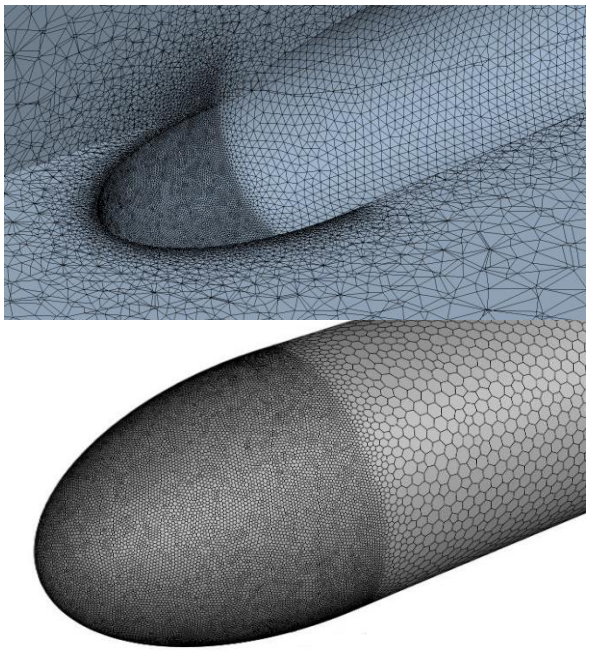

3.4 Boundary Conditions

The physical state of the solution domain has been represented by a set of boundary conditions shown in the Table 3.2 using mathematical conditions imposed at various physical locations in the domain. The k-ω SST turbulent model is used for modeling the turbulent simulation.

Table 3.2: Boundary conditions of CFD simulation

	No slip (Hull of vehicle-segment EF)	**Slip (Segment AD and BC)**	**Velocity Inlet (Segment AB)**	**Pressure Outlet (Segment CD)**
u	$u_i = 0$	$u_i n_i = 0, \frac{u_i}{\xi_B} = 0$	$u_i = constant$	$\frac{u}{\xi_B} = 0$

P	$\frac{P}{\xi_B} = 0$	$\frac{P}{\xi_B} = 0$	$\frac{P}{\xi_B} = 0$	P = 0
k	k = 0	$\frac{k}{\xi_B} = 0$	$k = constant$	$\frac{k}{\xi_B} = 0$
ω	$\omega = f(u_r, \dots)$	$\frac{\omega}{\xi_B} = 0$	$\omega = constant$	$\frac{\omega}{\xi_B} = 0$

In the above table, u_i represents time average velocity components in cartesian directions, n_i represents normal to surface, ξ_B represents parameter direction crossing the boundary, k represents turbulent kinetic energy, ω represents specific dissipation of turbulent kinetic energy and P represents time average pressure.

3.5 Solver Parameters

For the CFD simulations of the glider, the FLUENT solver of ANSYS was used to solve steady state RANS equations. The convective and explicit terms are used for application of second order explicit defect correction to approach second order accuracy. No slip condition is applied to the walls and glider surface. Report generation feature is used to monitor the lift and drag coefficients on the glider surface throughout the simulation iterations until convergence is achieved. Computations are carried out for 1000 iterations but converged at 170, so the max iterations are reduced to 200 with artificial timestep of 0.1 s.

The simulations are done at three glider velocities (0.25, 0.5 and 1.0 m/s), 7 angle of incidences (-9^o to 9^o in steps of 3) and 11 angle of attacks (-60^o to 60^o in varying steps) for all three velocities. The drag and lift coefficients in steady state condition are measured for each of the simulations and tabulated in the results below.

3.6 CFD Simulation Results

The data is plotted in several methods as shown below.

The Figure 3.5 shows the hydrodynamic coefficients at the range of angle of attack at three velocities (0.25, 0.5, 1.0 m/s) and at 0 degree angle of incidence (angle of wings with respect to the main body).

Figure 3.5: Drag, Lift and Pitching moment Coefficients at 3 velocities as function of Angle of Attack

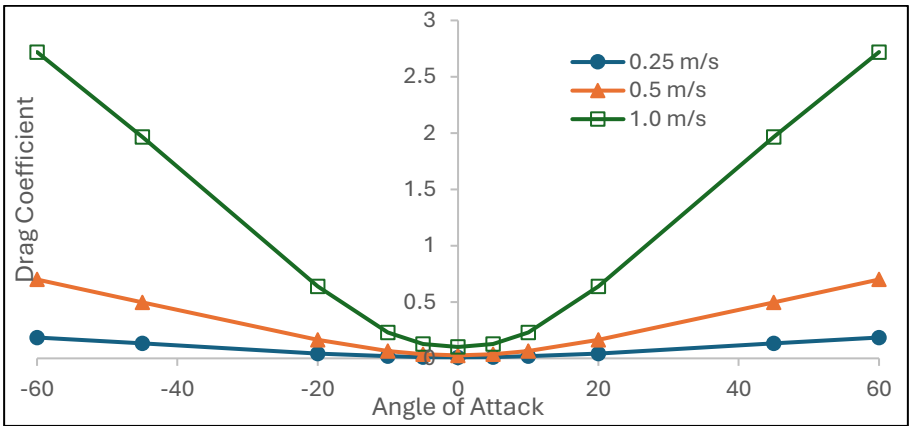

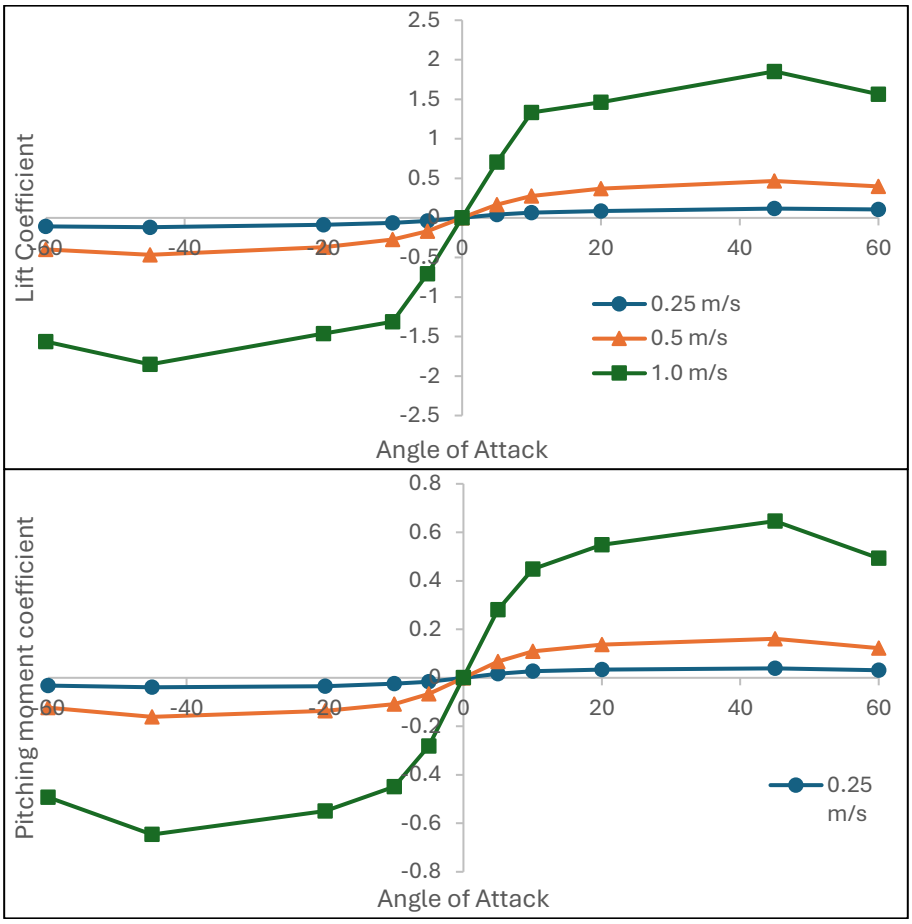

The Figure 3.6 shows the variation of hydrodynamic coefficients with respect to the range of Angle of incidence (wing angle) at a constant angle of attack of 0 degree.

Figure 3.6: Drag, Lift and Pitching moment Coefficients at 3 velocities as function of Angle of Incidence

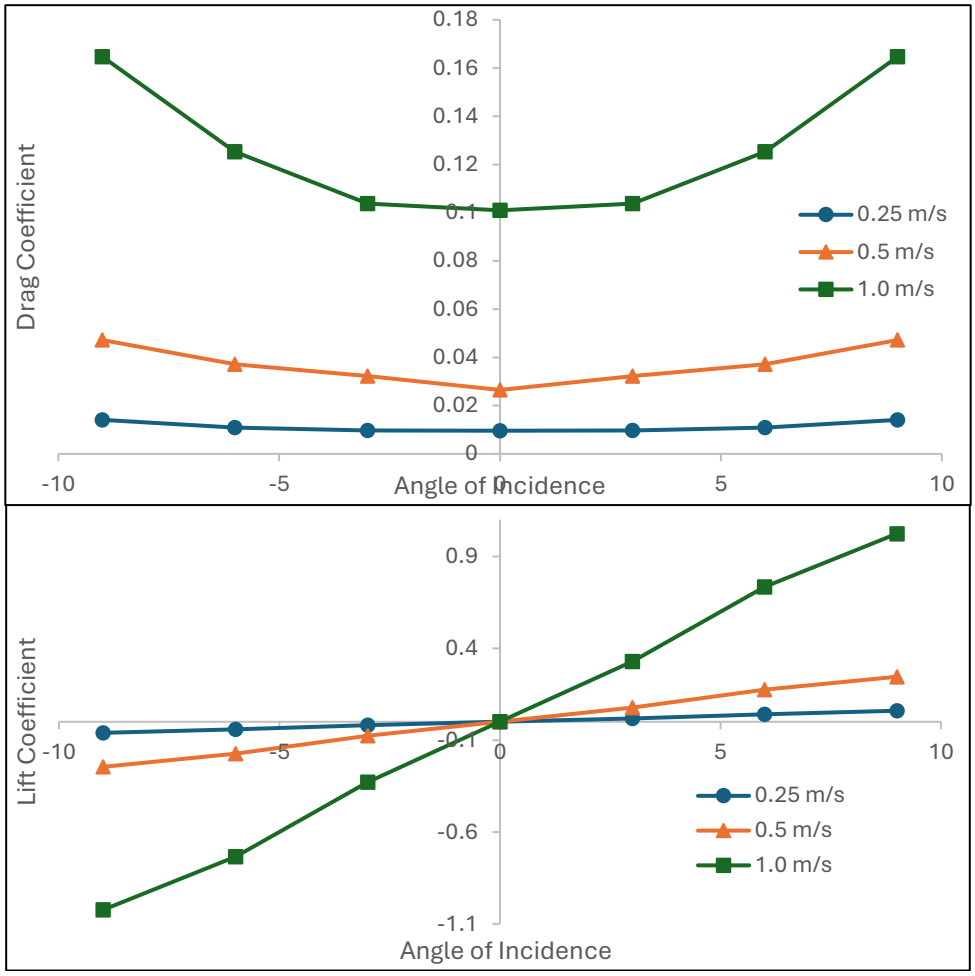

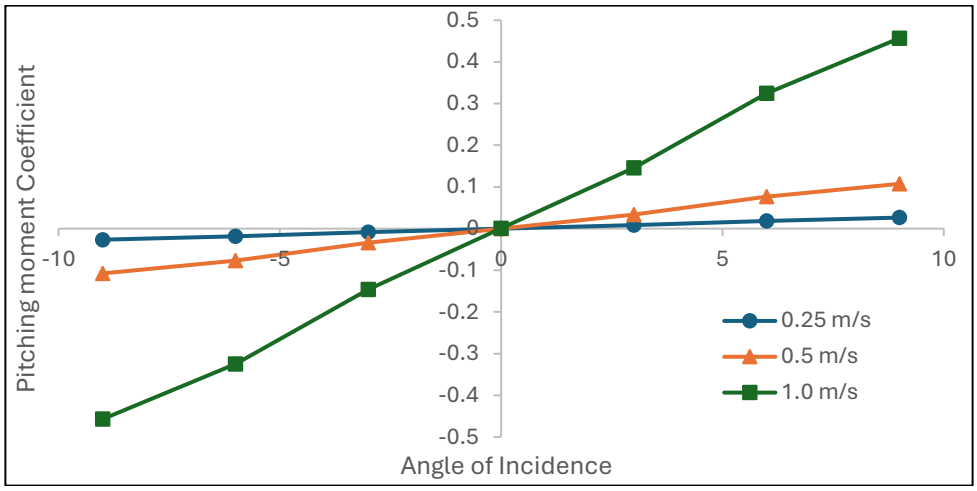

The Figure 3.7 shows the combined effect of the lift and drag coefficients in the form of Lift to Drag ratio as a function of both, the Angle of Incidence and the Angle of Attack in a 3D plot. The values are also tabulated below in Table 3.3.

Table 3.3: Lift to Drag ratio as dual function of Angle of attack and incidence

L/D Ratio		**Angle of incidence**			
		0	3	6	9
Angle of attack	0	0.010	3.162	5.863	6.217
	5	5.549	5.814	4.692	3.520
	10	5.830	3.650	3.020	2.493
	20	2.284	2.043	1.865	1.697
	45	0.942	0.893	0.833	0.780
	60	0.576	0.538	0.497	0.460

Figure 3.7: Lift to Drag Ratio 3D plot w.r.t Angle of attack and incidence

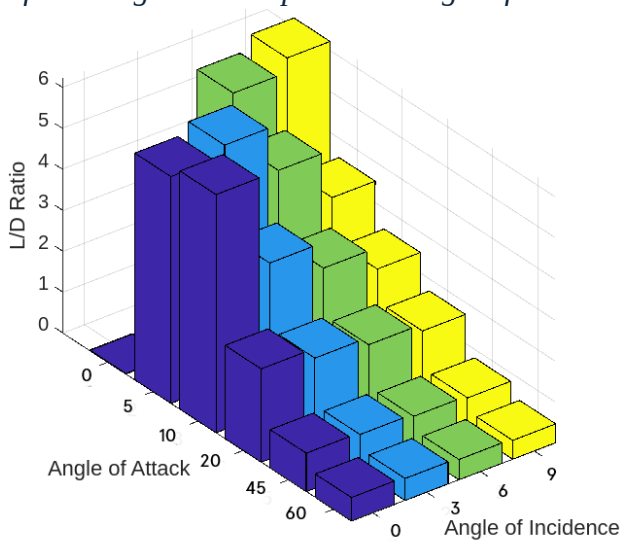

3.7 Conclusion from Results

This section establishes the CFD methodology for the computation of the lift and drag forces on the glider by varying its angle of attack and wing angle in different gliding speeds. The results show that both the drag and lift forces increase rapidly with increasing angle of attack as well as angle of incidence. At around 20^{o} angle of attack the drag is within a reasonable limit with a high lift creating a good L/D ratio. Above this angle the lift to drag ratio goes below 1, which indicates that this is the stall condition and operating at this gliding angle will decelerate the glider horizontally and instead of gliding forward the glider will start moving backwards and will loose control. This point is essential in establishing the pitch control system in the later stages of the project when the moving

mass fixed in the glider changes the center of gravity of the glider to adjust the trim of the glider after the buoyancy center has been changed by the buoyancy engine.

It is also observed that till angle of attack of 20^o, apart from 0^o angle of attack, the increasing angle of incidence has a negative effect, as it can be observed from the decreasing lift to drag ratio. So, it was decided that the final glider model will have no/neutral wing angle according to these results.

CHAPTER 4: DESIGN CALCULATIONS & FEA ANSLYSIS

4.1 Buoyancy:

A buoyancy-driven underwater glider uses a variable-volume system to control its buoyancy. The depth of the underwater glider is determined by three buoyancy conditions acting on the gliders that are dependent on the net force acting on the glider. When the buoyancy force is less than the gravitational force acting on the glider, the glider sinks in the water. Similarly, when the buoyancy force is greater than the gravity force, the glider rises. When both of these forces balance each other, the glider is neutrally buoyant and maintains its depth.

The volume of the glider was determined using the CAD model in SolidWorks, whereas the mass of water displaced for each buoyancy condition was determined by the variable-buoyancy system of the glider, since it stores and releases water according to the requirement. By using the volume of glider, the buoyancy force was calculated using the formula:

$$F_B = \rho V g$$

Where ρ is the density of water and g is the value of gravitational acceleration.

$$Volume\ of\ Glider = 0.0085 m^3$$

$$Density\ of\ Water = 1000 kg/m^3$$

The calculated results for all three buoyancy conditions are shown in the table below:

Table 4.1: Net force on glider in different buoyancy conditions

Buoyancy Condition	**Mass of Water Displaced (kg)**	**Buoyancy Force (N)**	**Net Force**
	$m = \rho V$	$F_B = \rho V g$	$F_{Net} = F_B - F_G$
Negative	8.65	84.83	1.47
Neutral	8.5	83.36	0
Positive	8.35	81.89	-1.47

4.2 O-Rings:

An O-ring is a torus-shaped ring, typically made from an elastomer material that is used to prevent the loss of fluid or gas. The underwater glider requires the use of sealing equipment to prevent water from entering the hull and damaging the electrical equipment of the glider. The selection of O-rings as a sealing mechanism was primarily due to their sealing capabilities across a wide range of temperature and pressure. Moreover, they are lightweight, cost-effective, and durable.

The male design places the groove and O-ring on the piston. This may also be called a piston seal. A variation of this is the female design, which places the groove inside the bore. This may also be called a rod seal the purpose of groove is to support the O-rings. The O-ring used in our underwater glider is a static piston seal with a male groove. The durometer hardness number for O-rings is 70, which are suitable for applications with a pressure of up to 800 kPa. The standard used for the design calculations of O-rings is the US AS568 standard. By using the known dimensions of our glider, the dimensions of O-ring features such as the groove outer diameter, O-ring inner diameter, and cross-sectional diameter were determined.

$$Cylinder\ Bore\ Internal\ Diameter\ =\ 111\ mm$$

Using the US AS568 Standard,

$$Groove\ Outer\ Diameter\ =\ 104.5\ mm$$

$$Piston\ Outer\ Diameter\ =\ 111\ mm$$

$$O-ring\ Inner\ Diameter = G_d(1 - S_{rec})$$

$$O-ring\ Inner\ Diameter = 104.5(0.98) = 102.4\ mm$$

Here, G_d is the groove diameter and S_{rec} is the recommended stretch. Its value is 2% (or 0.02).

$$Cross-Section\ Diameter\ =\ \frac{B_d - G_d}{2(1-C)}$$

$$Cross-Section\ Diameter\ =\ \frac{111 - 104.5}{1 - 0.3}\ =\ 4.64\ mm$$

$$Groove\ Width = CS_{dia}(1.5) = 6.96\ mm$$

$$Groove\ Depth\ =\ 4\ mm$$

4.3 Torque Calculations:

The mechanism by which torque is provided from the stepper motor to the buoyancy engine consists of a coupling and a lead screw that connect the motor and variable-buoyancy system together. To determine whether the selected motor can provide sufficient torque to the syringes in the buoyancy system, the following calculations were made:

$$Lead\ of\ Screw\ =\ 0.004\ m$$

$$Diameter\ of\ Plunger =\ 0.031\ m$$

$$Number\ of\ Plungers\ =\ 5$$

$$NEMA\ 17\ Motor\ Torque\ =\ 0.45\ N.m$$

$$Area\ of\ Plunger = (\pi r^2) = 7.547(10^{-4})\ m^2$$

$$Lead\ Screw\ Efficiency\ =\ 60\%$$

Work done per turn by the motor is given by:

$$W\ = 2\pi T\eta = nA_pLP$$

Solving for pressure,

$$P\ =\ 112.4\ kPa$$

This is the pressure that the NEMA 17 stepper motor can apply to each syringe to push water out of the hull. At the depth of 10m, the external pressure is about 100 kPa, so the torque provided by the selected motor is adequate.

Figure 4.1: Torque delivery mechanism for variable buoyancy system

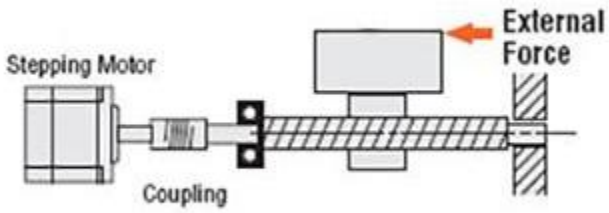

4.4 FEA Analysis:

4.4.1 Structural Analysis of Hull as a Pressure Vessel:

The hull of an underwater glider must be able to withstand the externa pressure exerted by water as it traverses at a certain depth. For this purpose, the structural analysis

of hull was carried out using ANSYS Static Structural. The hull is made of Unplasticized Polyvinyl Chloride (UPVC). The hull diameter is 4 inches (101.6 mm) with a length of 1000 mm. The glider is designed for a depth of 5 m where the water pressure is about 49 kPa. The structural analysis of hull was performed using Ansys Static Structural. For the analysis, the pressure applied on hull is 150 kPa as a factor of safety. For the first iteration the hull was analyzed as a hollow cylinder, whereas during the second iteration the hull was analyzed with baffles placed inside for structural support.

Figure 4.2: Properties of UPVC

Density	1.392e-06 kg/mm³
Structural	
Isotropic Elasticity	
Derive from	Young's Modulus and Poisson's Ratio
Young's Modulus	3600 MPa
Poisson's Ratio	0.335
Bulk Modulus	3636.4 MPa
Shear Modulus	1348.3 MPa
Isotropic Secant Coefficient of Thermal Expansion	0.0001273 1/°C
Tensile Ultimate Strength	46.71 MPa
Tensile Yield Strength	46.71 MPa

Figure 4.3: Cylinder Mesh

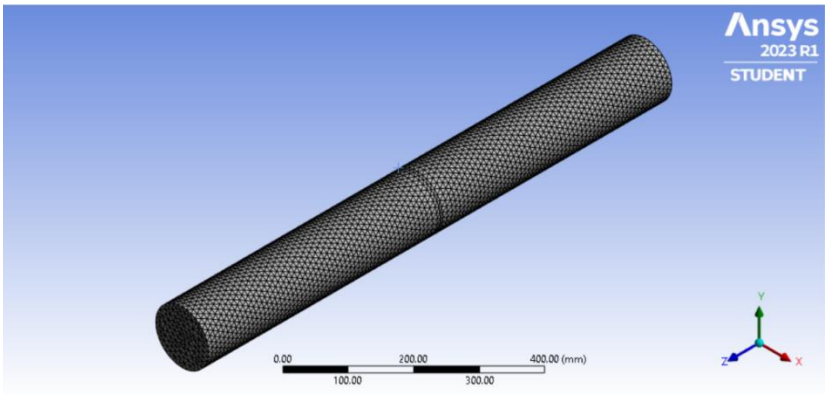

The boundary conditions imposed during the analysis are as follows:

- Fixed support on both ends.
- Pressure of 150 kPa acting normal to the Hull's cylindrical surface.

Figure 4.4: Boundary Conditions

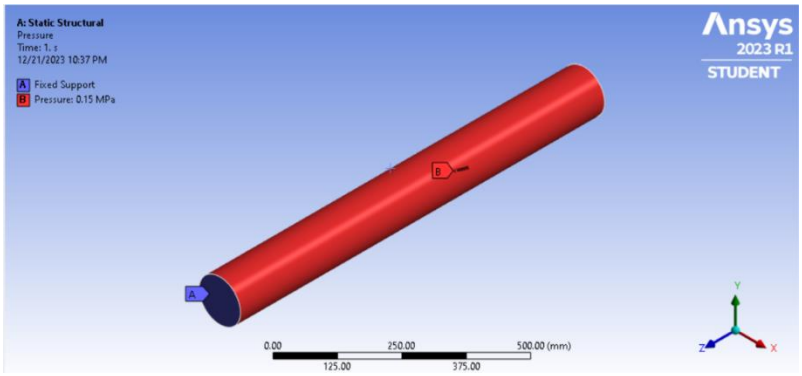

Figure 4.5: Total Deformation (Left) and Equivalent Stress (Right) for Hull without Baffles

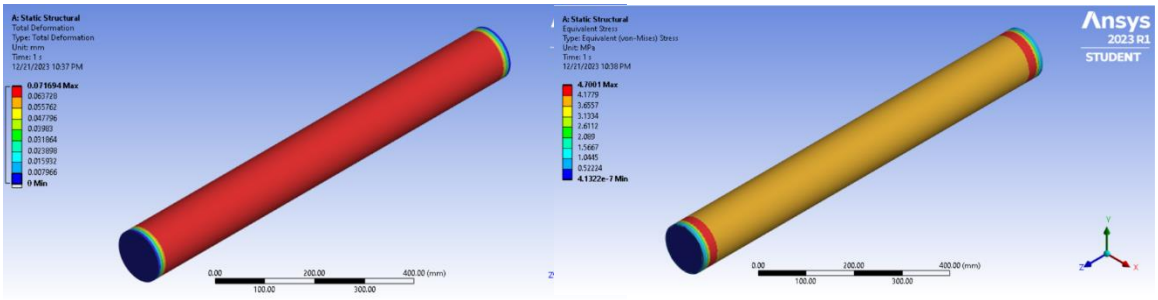

Figure 4.6: Total Deformation (Left) and Equivalent Stress (Right) for Hull with Baffles

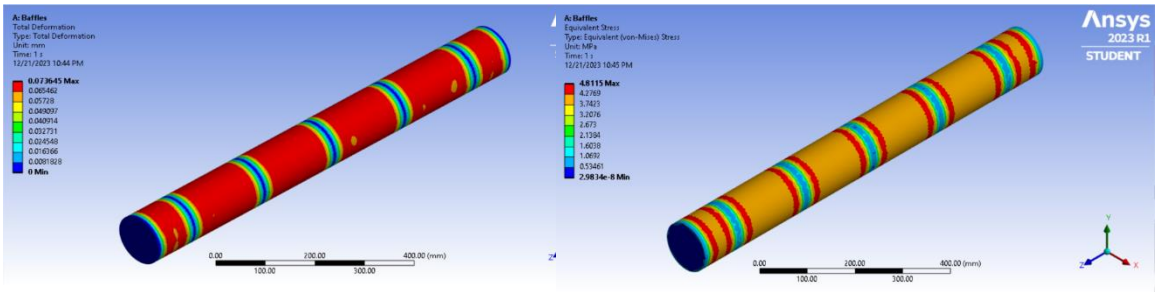

Table 4.2: Hull Structural Analysis Results

Iteration	Equivalent Stress (MPa)		Total Deformation (mm)	
	Max	Min	Max	Min

Without Baffles	4.700	4.132	7.169e-2	0
With Baffles	4.812	3.314	7.364e-2	0

4.4.2 Gravity Analysis of Wings:

To determine whether the wings can sustain their own weight under gravity when assembled with the glider, a load analysis was carried out by treating the wing as a cantilever beam. The simulation was performed using ANSYS Static Structural and the material used is Acrylic.

Figure 4.7: Properties of Acrylic

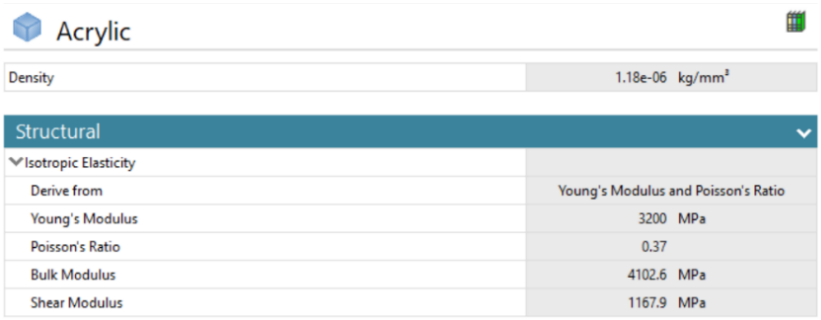

Figure 4.8: Wing Mesh

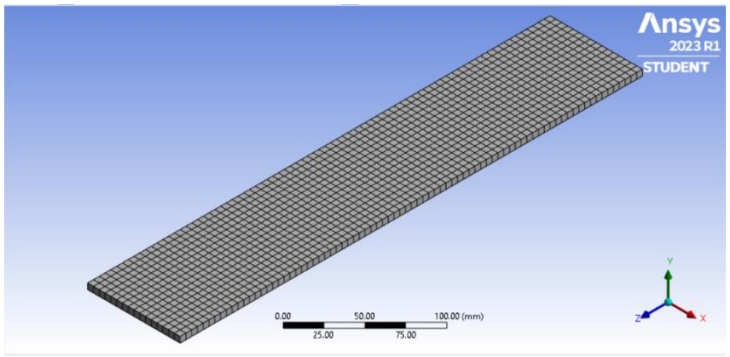

Two iterations were performed, one with a 5 mm thick wing while the other with a thickness of 8 mm. The boundary conditions imposed during the analysis are as under:

- Fixed support on one end of the wing.
- Gravity load on the wing.

Figure 4.9: Boundary Conditions

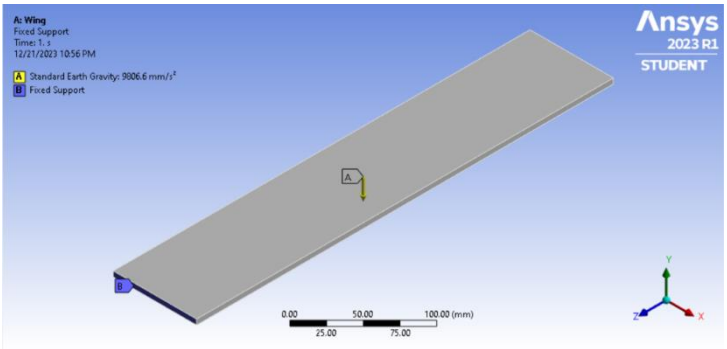

The results obtained as a result of the simulation are summarized below:

Table 4.3: Wing Gravity Analysis Results

Iteration	Directional Deformation (mm) (y-axis)		Total Deformation (mm)	
	Max	Min	Max	Min
5 mm Thickness	3.93e-4	-5.335	5.336	0
8 mm Thickness	3.162e-7	-2.093e-3	2.094e-3	0

Figure 4.10: Deformation of 5 mm Wing

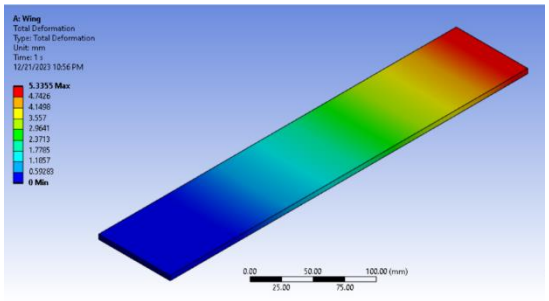

Figure 4.11: Deformation of 8mm Wing

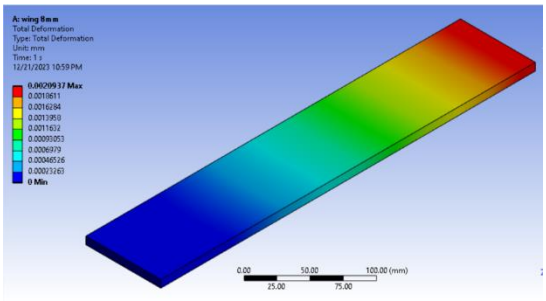

CHAPTER 5: 3D CAD MODELLING

This chapter establishes the design and models of the components used in the 3D model of our AUV glider keeping in view the calculations done in chapter 4. The extensive CAD model for our Underwater Buoyancy driven vehicle is given below.

5.1 Structural Model:

5.1.1 Hull Pipe:

Our AUV's hull is designed using available and cost-effective 4-inch diameter Series 40 UPVC pipe. This material offers a good balance of strength, affordability, and resistance to corrosion in saltwater environments, making it well-suited for underwater operation. With a wall thickness of 1.5mm and a total length of 0.9 meters, the pipe provides ample volume for internal components while maintaining a streamlined profile that minimizes drag in the water.

Figure 5.1: UPVC Hull Pipe

5.1.2 Nose:

The AUV's nose has a streamlined elliptical shape for optimized water flow and reduced drag. This 3D printed component prioritizes both functionality and efficiency. Five

holes allow for water intake through syringes. An additional dedicated hole houses a pressure sensor, providing crucial data on depth and movement.

Figure 5.2: 3D Printed AUV Nose with holes for ballast system

Figure 5.3: 3D Printed Tail

5.1.3 Tail:

The 3D-printed tail of our AUV ensures stability and maneuverability. Its vertical stabilizer provides directional control, while a designated rudder placement can be made which will allow fine-tuning and precise movement.

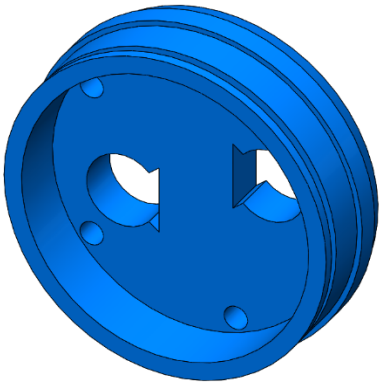

Figure 5.4: Acrylic Sheet Wings

5.1.4 Wing:

The AUV's wings, crafted from an 8mm acrylic sheet, has a sleek 350mm x 80mm profile. This design ensures rigidity while minimizing drag, optimizing underwater stability and lift. The generous wingspan contributes to buoyancy and control, making the AUV adept at maneuvering through its aquatic environment.

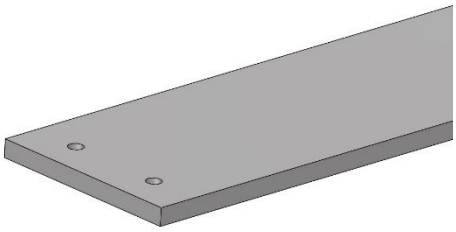

5.1.5 Wing Mounts:

The AUV's 3D printed wing mounts ensure the secure and efficient attachment of the wings to the hull. Their design, while not visible in the provided image, likely prioritizes both strength and minimal drag to optimize performance.

Figure 5.5: 3D Printed Wing Mounts

5.2 Buoyancy Engine:

5.2.1 Syringes:

Five 60cc syringes are strategically positioned within the AUV, form the core of its buoyancy engine. These components displace a total of 150cc, equivalent to 150g of water towards one direction (upward or downward motion), allowing precise control over the AUV's vertical movement. Their neutral placement in the middle position enables both upward and downward maneuvers, ensuring efficient navigation through varying depths.

Figure 5.6: 60 ml syringe

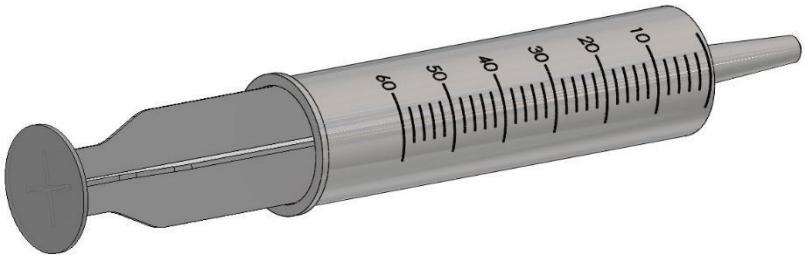

5.2.2 Lead Screw assembly:

A ball screw, coupled to a lead screw, translates rotational motion into smooth linear displacement, driving the syringe plates responsible for buoyancy adjustment. An

M6 rod adds structural integrity and stability to this assembly, ensuring reliable operation under varying water pressures.

Figure 5.7: Lead Screw Assembly

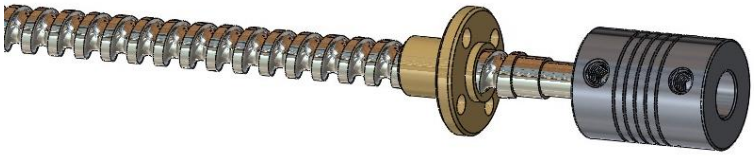

5.2.3 Limit Switch:

Figure 5.8: Limit switch

A limit switch is placed within the AUV. It functions to control the motion of the syringes. It triggers to keep the syringe motion within the predefined region. It is connected to the motor and gives a signal whenever triggered.

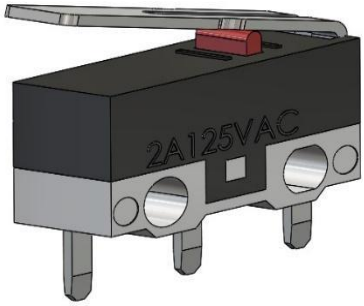

5.2.4 NEMA 17 Stepper Motor:

Figure 5.9: NEMA 17 Motor

The buoyancy engine uses a NEMA 17 stepper motor. This highly efficient powerhouse delivers both high torque and precise control, controllable rotations of the lead screw. With its flexible voltage range from 12V to 24V, it adapts seamlessly to the system's power requirements, ensuring reliable operation and manipulation of the syringe plates for optimal buoyancy control.

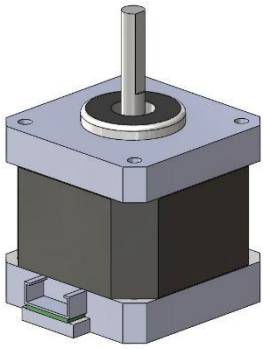

5.2.5 3D Printed Plates:

Five 3D-printed plates form the backbone of the syringe system, ensuring each 60cc syringe is securely placed and precisely positioned. Their design allows for individual syringe control and fine-tuning of buoyancy adjustments. The plates' interaction with the lead screw enables smooth, coordinated movement, optimizing the AUV's vertical navigation.

Figure 5.10: 3D Printed Plates

5.3 Pitch Control:

5.3.1 NEMA 17 Stepper Motor:

The AUV's pitch control system, crucial for maintaining precise underwater heading, utilizes a NEMA 17 stepper motor as its driving force. This motor, known for its high torque and efficiency, ensures the lead screw smoothly translates rotational motion into linear displacement. A precise nut and coupler arrangement further ensures accurate translation for fine-tuning pitch angles.

5.3.2 Sliding Assembly:

The 3D-printed sliding assembly is integral to the AUV's precise pitch control. This component houses the battery, acting as the primary weight for adjusting pitch angle. An additional compartment offers the flexibility to add more mass, allowing for fine-tuning and balancing based on specific mission requirements. It moves in horizontal direction with the help of the motor for fine pitch control.

Figure 5.11: Sliding Mass Assembly

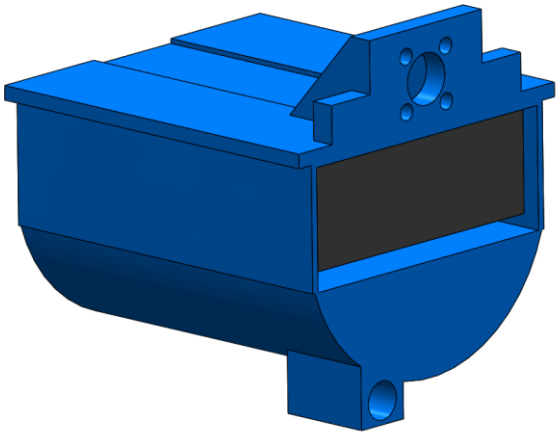

5.3.3 M6 Rod:

M6 rods are used here for the structural integrity and stability of the AUV. Their resistance to bending and deformation allows the system to perform its functions smoothly.

5.3.4 Plates:

Two 3D plates are used in the pitch control system of the AUV just like the ballast system. These plates hold this assembly together with the help of 3 M6 threaded rods and the threaded rods also provide linear sliding support to the sliding assembly during its motion.

5.4 Electronics:

The Arduino UNO serves as the AUV's control unit, coordinating all operations. For stable movements, pressure and angle sensors provide crucial data on depth and orientation, allowing the AUV to adjust buoyancy and maintain desired pitch. Wires help to make connections, transmitting signals throughout the system. Limit switches act as safeguards, halting operations when reaching specific limits. A reliable battery fuels the

AUV's journey, while dedicated controllers translate commands from the Arduino into precise instructions for individual components.

CHAPTER 6: PROTOTYPING & TESTING

This chapter outlines the procedure for assembling all components of the AUV glider to create a functional prototype. It details the sequential steps involved in the assembly process, from gathering individual parts to integrating them into a cohesive unit. Following assembly, the chapter delves into the testing phase aimed at validating the design and calculations. Through systematic testing procedures, the glider's performance and functionality are evaluated across various conditions to ensure its reliability in real-world scenarios. This thorough examination underscores our commitment to developing a robust AUV glider capable of meeting the demands of underwater exploration and research.

6.1 Prototype development:

6.1.1 Buoyancy Engine Assembly:

The buoyancy engine, alternatively referred to as the ballast system, serves as a pivotal mechanism for managing the buoyancy force that influences the vertical movement of the AUV glider. Its primary function is to regulate the glider's ascent or descent within aquatic environments. This is achieved through the controlled intake and release of water from the surrounding environment.

When the buoyancy system draws water into the glider, the added weight causes it to descend, effectively controlling its downward motion. Conversely, expelling water from the glider reduces its weight, enabling it to ascend. This dynamic adjustment of buoyancy ensures precise control over the glider's vertical movement, facilitating efficient navigation and maneuverability in varying aquatic conditions. The buoyancy system consists of:

- Syringes.
- 3D-printed plates.
- NEMA 17 motor
- Lead screw assembly.

Each syringe is of 60cc capacity, which are held together in place by two pairs of 3D printed plates. These plates are designed to control the movement of the syringes in a smooth manner. The NEMA 17 motor controls the motion of the syringes and is connected to the syringes via a lead screw assembly.

Figure 6.1: Buoyancy System

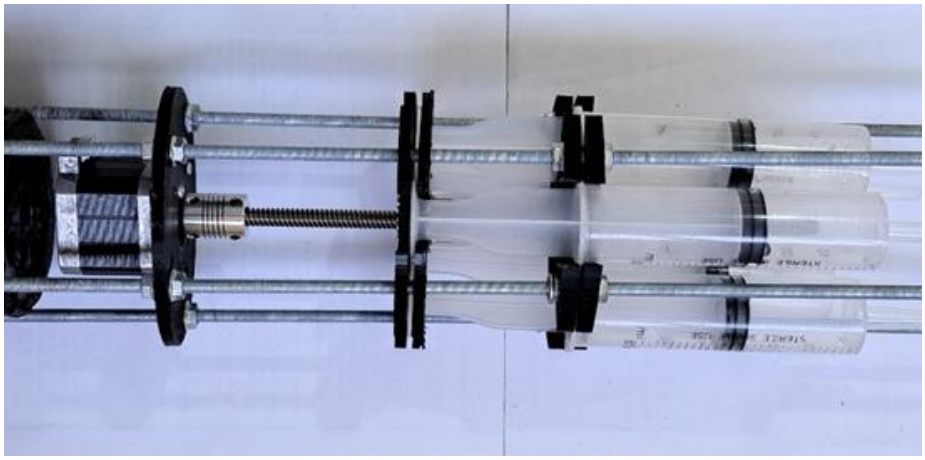

6.1.2 Pitch Control System:

The pitch control system plays a crucial role in managing the diving and ascending maneuvers of the glider. Central to this system is the NEMA 17 stepper motor, which operates in conjunction with a lead screw assembly. Together, they function as a mechanical powerhouse, precisely shifting a sliding mass assembly forward or backward.

The essence of this mechanism lies in its ability to influence the glider's center of mass through controlled movement. By strategically adjusting the position of the sliding mass, which ingeniously accommodates the glider's battery pack, the system generates a pitching moment. This moment effectively tilts the nose of the glider either upward or downward, enabling it to finely tune its diving angle and navigate along the desired underwater trajectory.

Figure 6.2: Sliding mass (Pitch Control System)

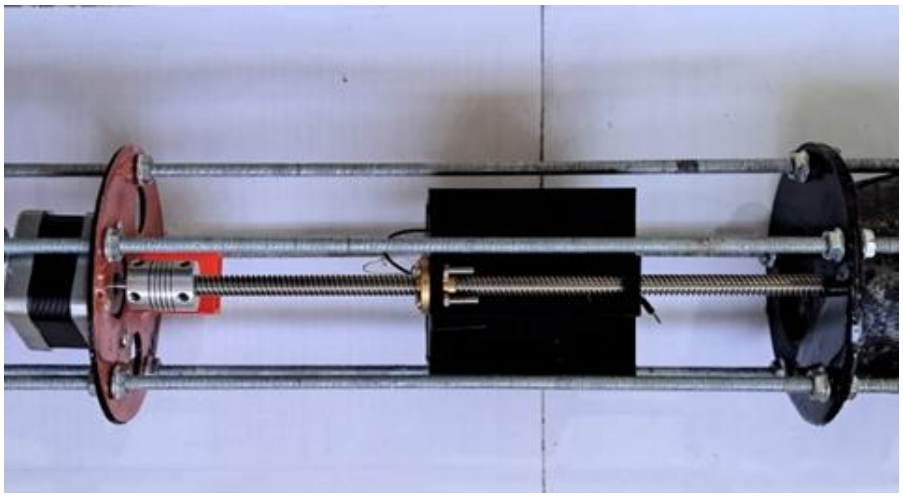

Additionally, the glider features a collection of fixed weights strategically positioned near its center of mass. These weights serve a dual purpose: firstly, they aid in stabilizing the glider, ensuring its equilibrium during operation; secondly, they contribute to increasing the overall weight of the glider. This deliberate addition of weight helps prevent the glider from floating atop the water's surface, particularly in situations where achieving neutral buoyancy might otherwise be challenging due to insufficient mass.

Figure 6.3: Fixed Weights

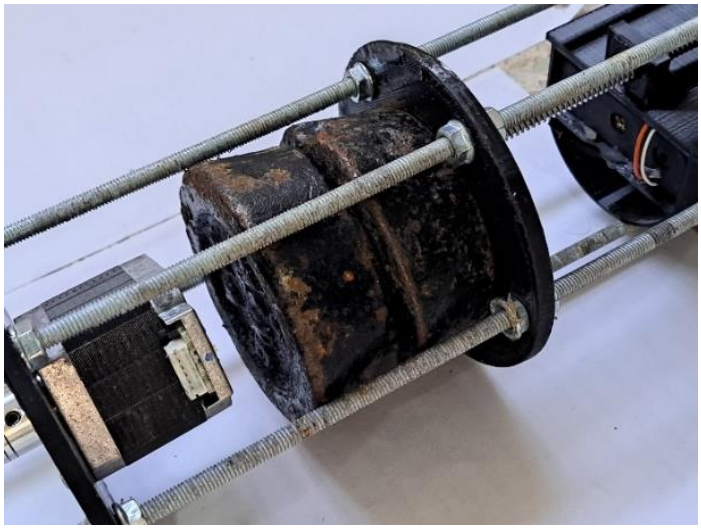

6.1.3 External features of AUV:

The AUV's external structure boasts a design that blends strength with adaptability to meet the demands of underwater exploration. The primary body of the AUV is crafted from Unplasticized Polyvinyl Chloride (UPVC), known for its robustness and resistance to water pressure and corrosion. This choice of material ensures a sturdy foundation for the glider's operations, enhancing its durability in challenging aquatic environments.

In contrast, the nose and tail sections of the AUV feature a shift in design to 3D-printed Polylactic Acid (PLA). This lightweight material facilitates more streamlined shaping, reducing drag and enhancing maneuverability in the water. The incorporation of PLA in these sections optimizes the AUV's performance, allowing for swift and agile navigation through underwater currents.

To further augment buoyancy and stability, the AUV's wings are meticulously crafted from 8mm thick acrylic sheets. These wings serve as essential components,

providing the necessary lift and balance for the glider during operation. To ensure seamless integration, custom-designed 3D-printed brackets are utilized to securely mount the wings onto the main body of the AUV. This assembly process results in a cohesive and functional external form, optimizing the AUV's performance and reliability in underwater missions.

Figure 6.4: Nose (Outside View)

Figure 6.5: Nose (Inside View)

Figure 6.6: Wing Mounts

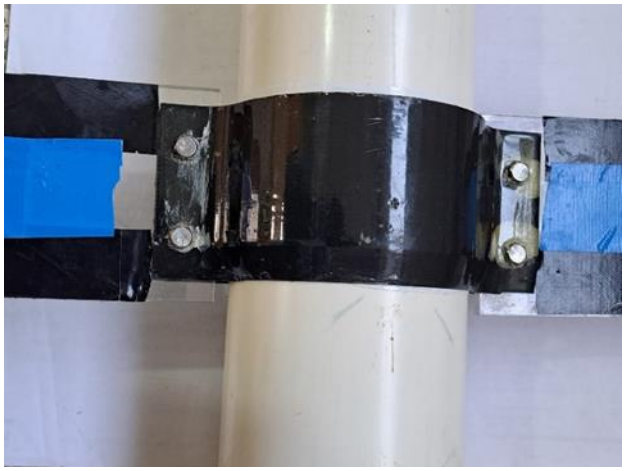

Figure 6.7: Tail Section (Outside View)

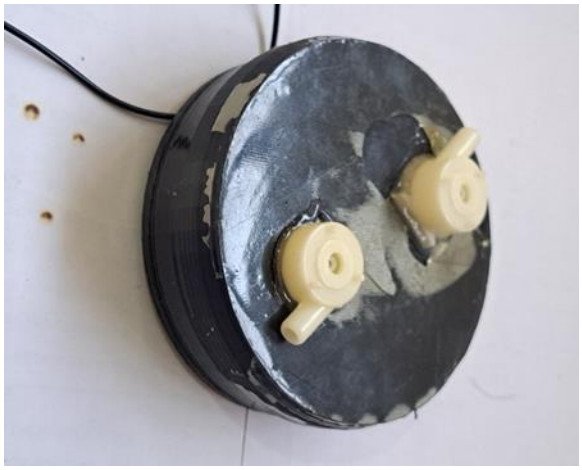

Figure 6.8: Tail Section (Inside View)

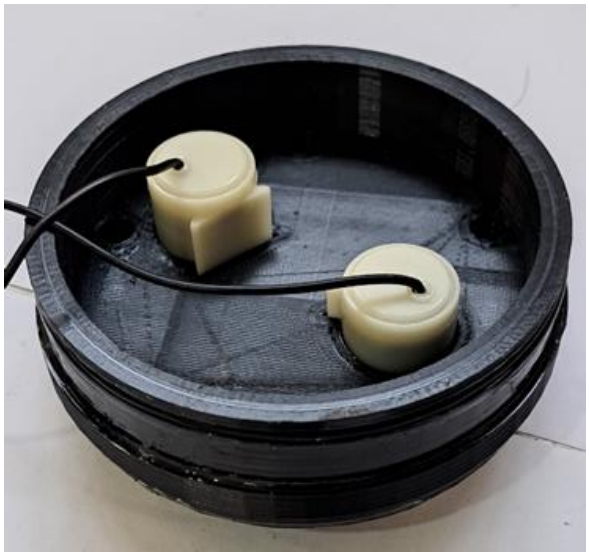

6.1.4 Final Assembly:

During the final assembly phase, we integrated the pre-tested subsystems – including the buoyancy engine, pitch control system, and other auxiliary components – into a fully functional AUV. To ensure the structural integrity of the control system and its optimal placement within the pressure vessel, we utilized a combination of rods and custom-designed 3D printed plates. These components formed a robust internal framework that securely housed the system's electronics.

Following the creation of the structural framework, we meticulously positioned all electronic components within the pressure vessel, establishing proper electrical connections to ensure reliable operation. Achieving neutral buoyancy, a crucial consideration for underwater navigation, was accomplished by strategically adding calibrated weights to the glider assembly.

With the internal components securely in place and appropriately weighted, the final assembly stage involved the attachment of the nose and tail sections to the main glider body. To guarantee watertight integrity, comprehensive sealing procedures were implemented at all connection points. This crucial step serves to safeguard the onboard electronics from potential water ingress during underwater operations.

Figure 6.9: Inside Structure of AUV

Figure 6.10: Inside Structure of AUV (2)

6.2 Electrical & Control Systems:

The electrical system of the glider comprises of the following major components:

Table 6.1: List of Electrical Components

Component	**Specification**	**Quantity**
Stepper Motor	NEMA 17	2
Stepper Motor Driver	A4988 Arduino Sheild	2
Microcontroller	Arduino UNO	1
Battery	12V Power supply	1
Limit switches		2
Pushbuttons		4
Gyroscope	MPU6050 Arduino Shield	1
Pressure Sensor	MPX5700 Arduino Shield	1
Relay		2
Water Pump		2
Wires, Resistors, Breadboard		As needed

The circuit schematic is shown in the diagram below.

Figure 6.11: Schematic Diagram of the Circuit system

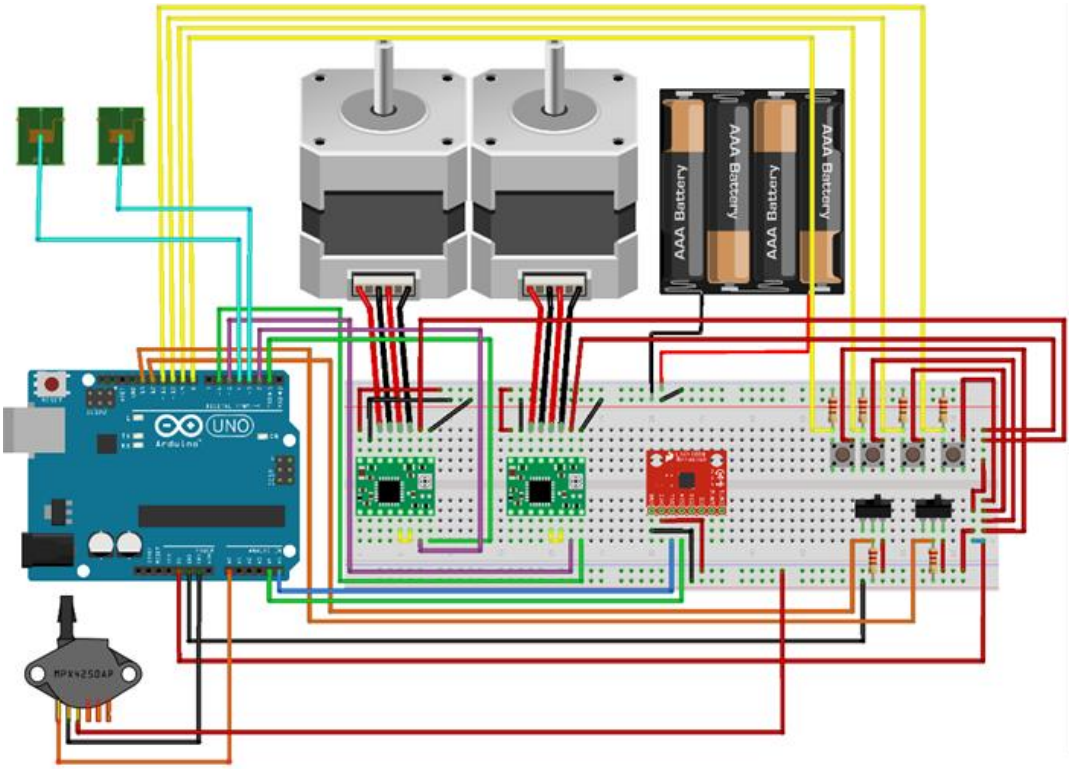

The stepper motors are used in the ballast and moving mass assemblies for powering the power screws. The drivers are used to give them input through the Arduino UNO.

The limit switches are used to identify the position of the assemblies' moving elements at the start of the operation. The motors are given input to move both the syringes and the moving mass to the very back of their range of motion where the limit switches are fixed. When the switch gets pressed, the controller knows that the moving element is at the end of its range and its location is set to 0 in the code so that it can be tracked easily moving forward from here. After this, whenever any one of the two motors is rotated, the position of the element is also tracked within the code. This is done by knowing that one rotation of the power screw gives 12 mm travel (this is called the lead of the power screw), and one rotation of the stepper motor has 200 steps (1.8 degree per step), so it's easy to update the

distance traveled by updating position after giving each step to the motor. This tracking of the moving parts helps make sure that they don't get moved out of their range, breaking the assembly or damaging any sensitive parts.

The pressure sensor, as previously described in the working principles, takes the raw voltage readings, converts them to pressure values within the microcontroller using the transfer function provided by the manufacturer, which is then converted to water depth in meters using Archemedes' Principle. This value is then utilized to program its zig zag motion within the set depths as explained in the working principles.

The Gyroscope, i.e., the MPU6050 is an IMU, or inertial measurement unit, device. It is a six-axis motion tracking gadget that computes data from a three-axis gyroscope and accelerometer. Its gyroscope and accelerometer unit is utilized to calculate the angle of the pitch of the glider using the following formula derived from basic trigonometry:

$$\theta_{pitch} = \text{atan}\left(\frac{A_{cc_Y}}{\sqrt{A_{cc_X}^2 + A_{cc_Z}^2}}\right)$$

This angle is continuously tracked within the disced and ascend. The optimal angle derived for max lift generated at the wings was calculated in the CFD analysis earlier, which turns out to be around 20 degrees. The pitch angle is measured continuously and using the moving mass assembly, the center of gravity is adjusted by moving the stepper motor to adjust the angle and keep it as close as possible to the optimal dive or rise angle (-20^o or 20^o respectively).

The pushbuttons are used to initiate several working steps of the glider, like initiating the calibration of position of the stepper motors, calibrating pressure and angle sensors and so on.

The relays are connected to water pumps which are used as water jets on the back side of the glider to provide turning moment when needed.

6.3 Prototype Testing:

6.3.1 Buoyancy Engine Testing:

The initial phase of testing focused on verifying the functionality of our custom-designed buoyancy engine. This critical component, comprised of five 60cc syringes, 3D-printed plates for structural integrity, stainless steel rods for reinforcement, a stepper motor, a threaded rod connected to the motor with a coupler, and interconnecting tubes, plays a vital role in regulating our AUV's buoyancy.

Following the assembly, the buoyancy engine underwent a submersion test in a controlled environment. Upon activating the stepper motor, we observed the successful actuation of the syringes. The pistons cycled smoothly, pumping water in and out, demonstrating the engine's ability to precisely manipulate the AUV's buoyancy. This successful test provided strong validation for our design and fabrication processes.

Figure 6.12: Buoyancy Engine

6.3.2 Weight Calibration and Sealing:

The second phase of testing addressed two crucial aspects: weight calibration to achieve neutral buoyancy and effective sealing to ensure watertight integrity. Our initial calculations estimated a total vehicle mass of 9 kg for submersion. However, upon submerging the assembled AUV in a swimming pool, we observed positive buoyancy, indicating insufficient weight. To rectify this, we systematically added weights in increments until the AUV achieved neutral buoyancy at precisely 12 kg.

Following weight calibration, we focused on achieving optimal center-of-gravity (CoG) placement, a critical factor for stable underwater maneuvering. Through adjustments in the placement of the added weights, we conducted multiple submersion tests and monitored the AUV's behavior. This iterative process culminated in achieving a stable CoG configuration, ensuring balanced underwater performance.

To complete the watertightness assessment, we implemented O-rings with pre-calculated specifications. These O-rings were strategically placed within designated grooves along the AUV's nose and tail sections. Subsequent submersion testing confirmed the effectiveness of the O-rings in preventing water ingress. As an additional safety measure, we applied duct tape to further reinforce the seals, safeguarding the sensitive electronic components housed within the AUV.

Figure 6.13: Weight Balancing

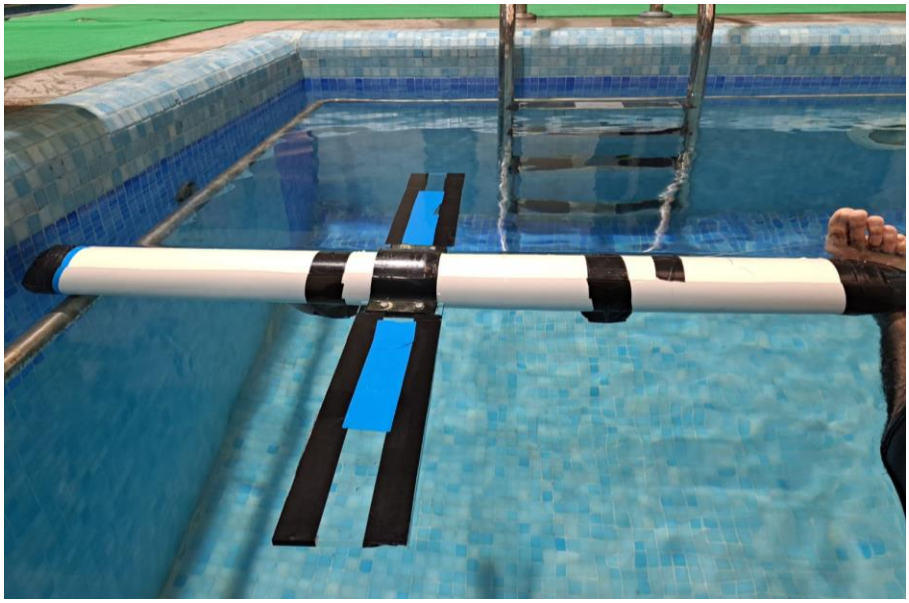

6.3.3 Path and Motion Control Testing:

The final phase of testing evaluated the AUV's ability to navigate a predetermined underwater path while maintaining programmed motion control. Given the limitations of the available swimming pool facility at NUST H-12, with a maximum depth of 12 feet, we designed a controlled test scenario tailored to these constraints.

Our AUV successfully executed its programmed 2-degree diving maneuvers within the confines of the pool. The diving and surfacing sequences corresponded precisely with our pre-determined calculations. We activated the AUV within the pool, initiating a controlled dive followed by the programmed expulsion of water from the syringes. This expulsion resulted in a positive buoyancy shift, causing the AUV to ascend, mimicking a sawtooth-like movement pattern.

For safety and operational control, a team member remained stationed within the pool alongside the AUV throughout the test. This proactive measure ensured immediate intervention capabilities in case of unforeseen circumstances.

Figure 6.14: Diving Glider

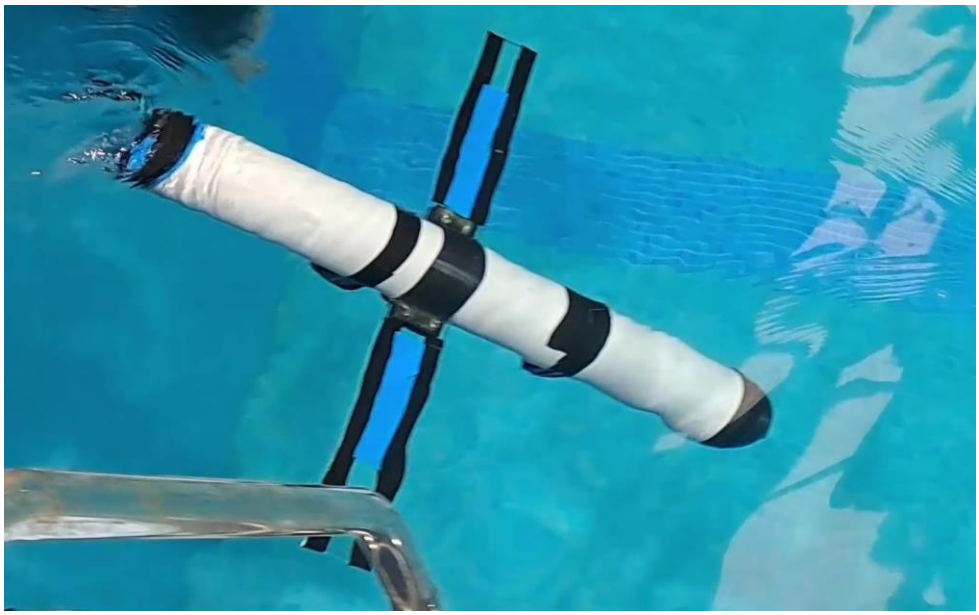

SUMMARY & CONCLUSION

The project achieved its primary objective of designing and analyzing an underwater glider, culminating in the development of a prototype to demonstrate the feasibility of a buoyancy-driven underwater vehicle. During the analysis phase, extensive studies were conducted on the fluid dynamics surrounding the glider, allowing for the observation and documentation of its performance characteristics under steady-state conditions, particularly in low-velocity water environments.

In the design phase, numerous calculations were undertaken to guide the development of various glider components, with computational tools utilized to enhance accuracy. An iterative approach was adopted during Computer-Aided Design (CAD) modeling to ensure compatibility with manufacturing processes, facilitating the seamless transition to the prototyping phase. Through this iterative process, a comprehensive model of the glider was developed, serving as a blueprint for procuring necessary parts and fabricating a functional prototype.

A portion of the glider's functionality was evaluated through testing in a swimming pool, where its operation and trajectory were observed. However, due to logistical constraints, the testing of the glider's turning motion using water jets could not be conducted as planned. Nonetheless, the innovative design developed for this purpose represents a novel approach not previously utilized in other buoyancy-driven underwater vehicles.

REFRENCES

[1] N. Ichihashi, M. Arima, & T. Ikebuchi. (2008). *Motion Characteristics of an Underwater Glider with Independently Controllable Main Wings*. IEEE.

[2] Bhattacharya, S., & Singh, Y. (2016). Design and Development of a Laboratory Underwater Glider.

[3] Webb, D. C., Simonetti, P. J., & Jones, C. P. (2001). SLOCUM: An Underwater Glider Propelled by Environmental Energy. In IEEE JOURNAL OF OCEANIC ENGINEERING (Vol. 26, Issue 4).

[4] Sherman, J., Davis, R. E., Owens, W. B., & Valdes, J. (2001). The Autonomous Underwater Glider "Spray." In IEEE JOURNAL OF OCEANIC ENGINEERING (Vol. 26, Issue 4).

[5] Eriksen, C. C., Osse, T. J., Light, R. D., Wen, T., Lehman, T. W., Sabin, P. L., Ballard, J. W., & Chiodi, A. M. (2001). Seaglider: A Long-Range Autonomous Underwater Vehicle for Oceanographic Research. In IEEE JOURNAL OF OCEANIC ENGINEERING (Vol. 26, Issue 4).

[6] Parker O-Ring Handbook ORD-5700 Retrived from https://www.parker.com/content/dam/Parker-com/Literature/O-Ring-Division-Literature/ORD-5700.pdf

[7] Huang, J., Choi, H. S., Vu, M. T., Jung, D. W., Choo, K. B., Cho, H. J., Anh, P. H. N., Zhang, R., Park, J. H., Kim, J. Y., & Tran, H. N. (2022). Study on Position and Shape

Effect of the Wings on Motion of Underwater Gliders. Journal of Marine Science and Engineering, 10(7).

[8] Armina, N. Ichihashi, & Y. Miwa. (2009). Modelling and Motion Simulation of an Underwater Glider with Independently Controllable Main Wings.

[9] Dong C. Seo, Gyungnam Jo, & Hang S. Choi. (2008). Pitching control simulations of an underwater glider using CFD Analysis. I E E E.

[10] Kan, L., Zhang, Y., Fan, H., Yang, W., & Chen, Z. (2007). MATLAB-based simulation of buoyancy-driven underwater glider motion. Journal of Ocean University of China, 7(1), 113–118.

[11] Wang, B., Xiong, J., Wang, S., Ma, D., & Liu, C. (2022). Steady motion of underwater gliders and stability analysis. Nonlinear Dynamics, 107(1), 515–531.

[12] Huang, J., Choi, H. S., Jung, D. W., Lee, J. H., Kim, M. J., Choo, K. B., Cho, H. J., & Jin, H. S. (2021). Design and motion simulation of an underwater glider in the vertical plane. Applied Sciences (Switzerland), 11(17).

[13] Stryczniewicz, K., & Drężek, P. (2019). CFD Approach to Modelling Hydrodynamic Characteristics of Underwater Glider. Transactions on Aerospace Research, 2019(4), 32–45.

[14] Sherman, J., Davis, R. E., Owens, W. B., & Valdes, J. (2001). The Autonomous Underwater Glider “Spray.” In IEEE JOURNAL OF OCEANIC ENGINEERING (Vol. 26, Issue 4).

[15] Jenkins, S. A., Humphreys, D. E., Sherman, J., & Org, E. (2003). Technical Report - Underwater Glider System Study

[16] Williams, S. B., Bender, A., Steinberg, D. M., & Friedman, A. L. (2008). Analysis of an autonomous underwater glider

[17] Davis, R. E., Eriksen, C. C., & Jones, C. P. (n.d.). 3. AUTONOMOUS BUOYANCY-DRIVEN UNDERWATER GLIDERS